S. Merkel

Université de Lille, France

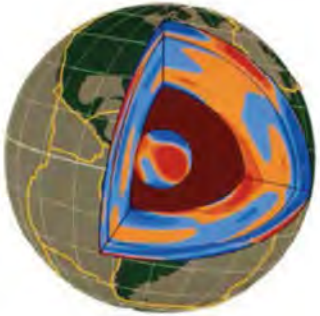

COLLÈGE DE FRANCE 1530

CHAIRE DE PHYSIQUE DE L'INTÉRIEUR DE LA TERRE
Année académique 2019-2020

Pr Barbara ROMANOWICZ

Global Scale Seismic Imaging and Dynamics of the Earth's Mantle

Colloque en anglais - Workshop in English
co-organised with Nicolas Coltice, ENS de Paris

Thursday October 7 and Friday October 8, 2021

Phase transitions in the mantle: effect on microstructures and seismic observables

Université de Lille

TIMEleSS ANR DFG

cnrs

TIMEleSS project

S. Merkel

C. Thomas

C. Sanchez Valle

S. Speziale

F. Rochira

J. K. Magali

M. Krug

E. Ledoux

J. Gay

WWU MÜNSTER

GFZ Helmholtz-Zentrum Potsdam

cnrs

Université de Lille

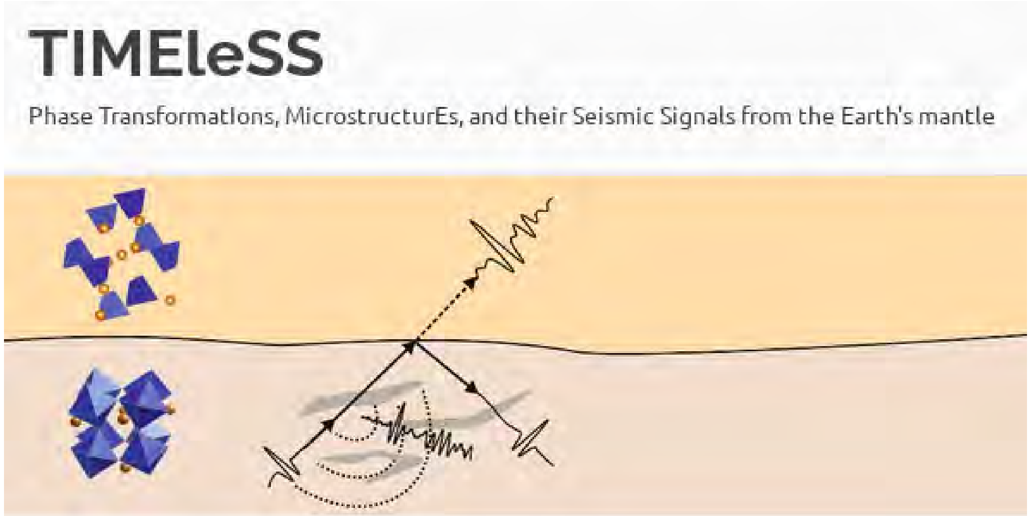

AGENCE NATIONALE DE LA RECHERCHE ANR

DFG Deutsche Forschungsgemeinschaft

In-situ study by multigrains crystallography of deformation of $(Mg,Fe)_2SiO_4$ wadsleyite at conditions of the 410 km depth discontinuity

E. Ledoux[1], J. Gay[1], M. Krug[2], O. Castelnau[3], J. Chantel[1], N. Hilairet[1], A. Fadel[1], M. Bykov[4], H. Bykova[4], G. Aprilis[4], V. Svitlyk[5], G. Garbarino[5], C. Sanchez-Valle[2], C. Thomas[6], S. Speziale[7], D. Jacob[1], S. Merkel[1]

1. Univ. Lille, CNRS, INRAE, Centrale Lille, UMR 8207 - UMET - Unité Matériaux et Transformations, F-59000 Lille, France
2. Institute for Mineralogy, WWU Münster, 48149 Münster, Germany
3. Laboratoire PIMM, UMR CNRS 8006, ENSAM, CNAM, 151 Boulevard de l'Hôpital, 75013 Paris, France
4 Deutsches Elektronen-Synchrotron DESY, Notkestr. 85, 22607 Hamburg, Germany
5 ESRF, the European synchrotron, 71 Avenue des Martyrs, CS40220, 38043 Grenoble Cedex 9, France
6. Institute of Geophysics, WWU Münster, 48149 Münster, Germany
7. German Research Centre for Geosciences GFZ, 14473 Potsdam, Germany

Geological context and topic

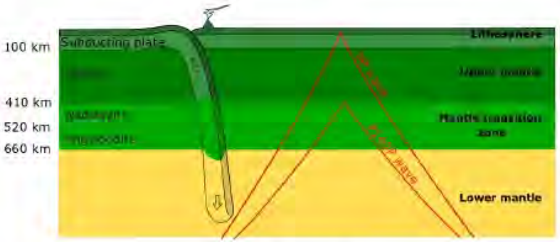

Earth's mantle transition zone :

- Dominated by wadsleyite (wd) in its upper part and by ringwwodite (rw) in its lower part
- Controls the sink or the stagnation of subducting slab
- Takes part in the global mantle convection
- Ellusive observations of seismic anisotropy
- Possible sources of anisotropy :
  - deformation-induced LPO of wd and/or rw
  - martensitic transformations of ol > wd > rw

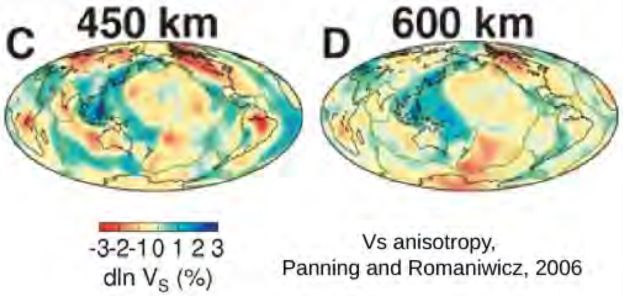

Vs anisotropy,
Panning and Romaniwicz, 2006

In this study, we investigate the plastic deformation of wadsleyite to test if it can be source of seismic anisotropy in the mantle transition zone

> first in-situ deformation study on dry wadsleyite at mantle transition zone pressures and temperatures

Microstructures Induced by Phase Transformations at the 660km Discontinuity

Jeff Gay[1], Estelle Ledoux[1], Matthias Krug[2], Anna Pakhomova[3], Julien Chantel[1], Carmen Sanchez-Valle[2], and Sébastien Merkel[1]

[1]Univ. Lille, CNRS, INRA, ENSCL, UMR 8207 - UMET - Unité Matériaux et Transformations, F-59000 Lille, France
[2]Institut für Mineralogie, Westfälische Wilhelms-Universität Münster, Münster, Germany
[3]Deutsches Elektronen-Synchrotron DESY, Hamburg, Germany

1. Introduction

- Phase transition from ringwoodite to bridgmanite in pyrolitic material responsible for seismic reflectors observed at 660 km depth
- Track mineralogical microstructures in-situ using Multigrain X-ray Diffraction (3D XRD)
  - Texture
  - Grain size distribution
  - Phase transformation

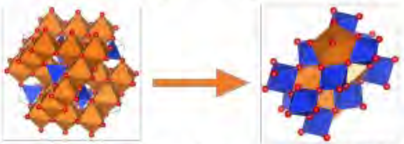

Figure 1. Phase transformation of cubic ringwoodite to orthorhombic bridgmanite.

- Combine mineralogical and seismological observations to model deep mantle processes
  - Identify origins of seismic reflectors
  - Effect of phase transitions of bridgmanite on slab subduction
  - Map deformation below 660 km discontinuity

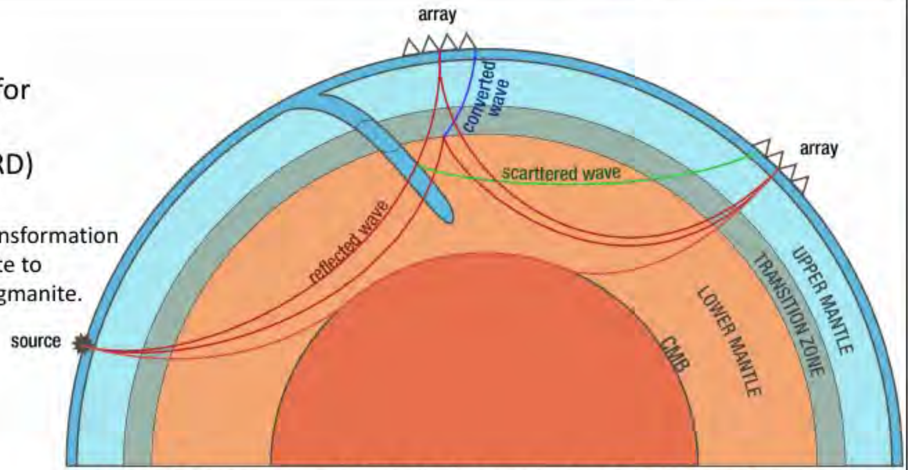

Figure 2. Cross section of Earth displaying seismic reflectors at various depths within the mantle.

Phase transformations in the mantle

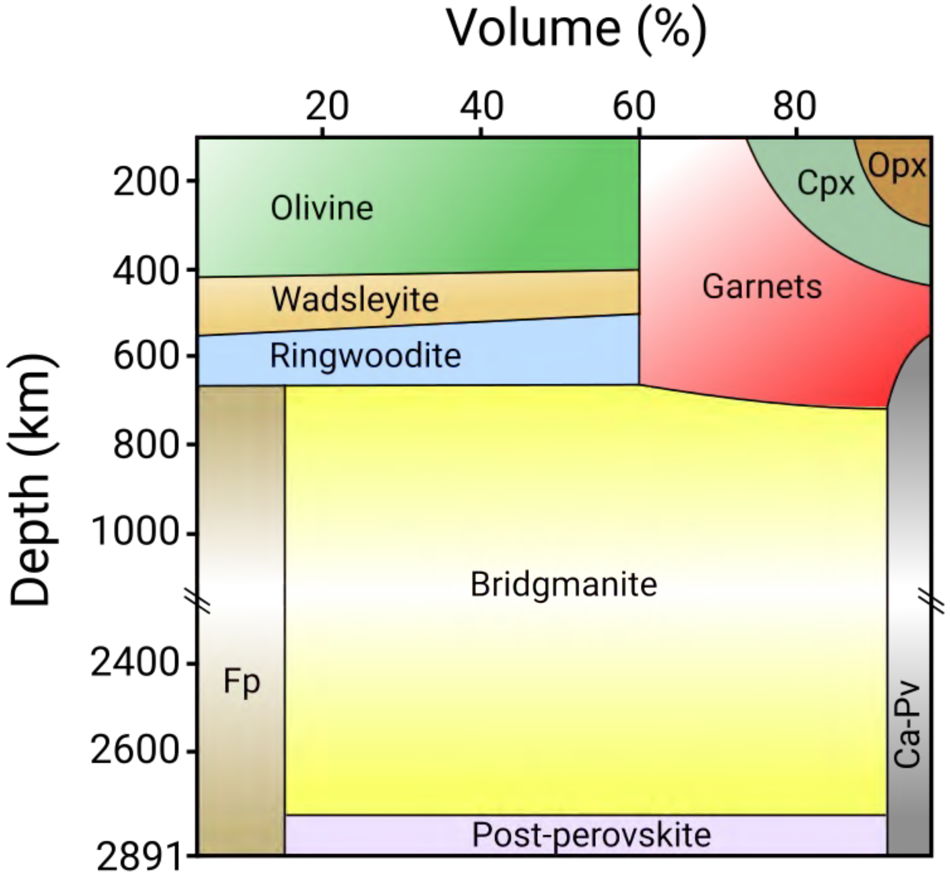

Cpx: clinopyroxene
Opx: orthopyroxene
Fp: ferro-periclase
Ca-Pv: calcium-perovskite

Main phase transitions in a pyrolitic composition

410 km: olivine to wadsleyite

520 km: wadsleyite to ringwoodite

660 km: ringwoodite / garnet to bridgmanite + ferropericlase + Ca-perovskite

D”: bridgmanite to post-perovskite

Phase transformations and seismic observations

Sharp transition of physical properties

- Reflectors
- Wave conversions

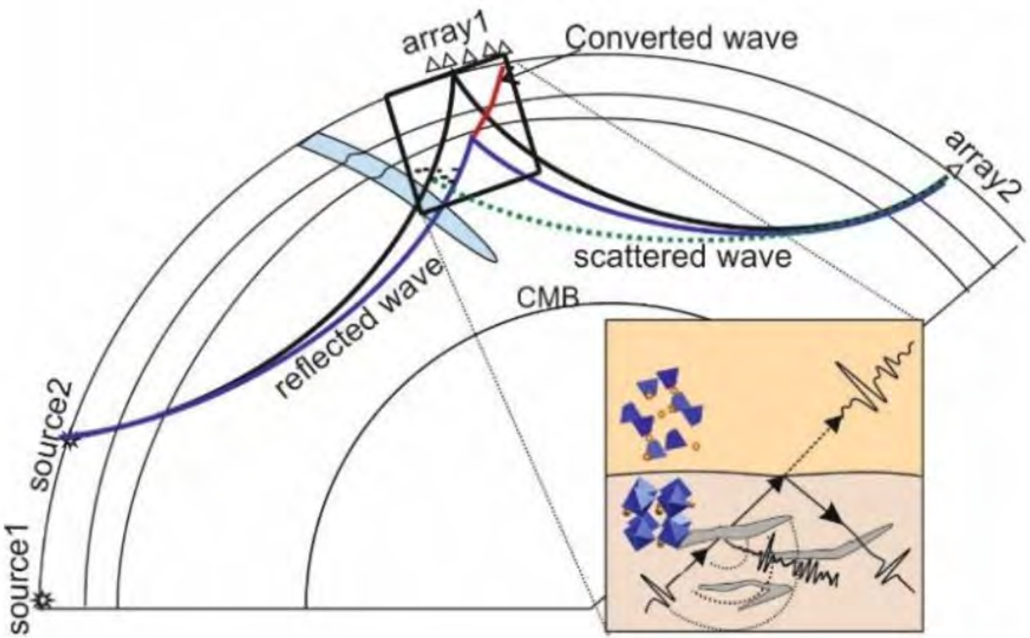

Microstructural imprint

- Anisotropy before and after the phase transformation
- Waveform and polarity of reflected / converted waves

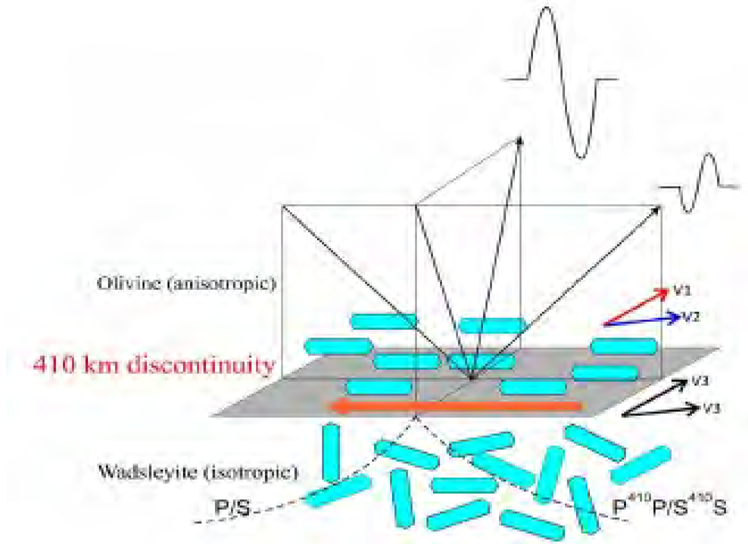

Phase transitions detectability

Wave reflections atop D”

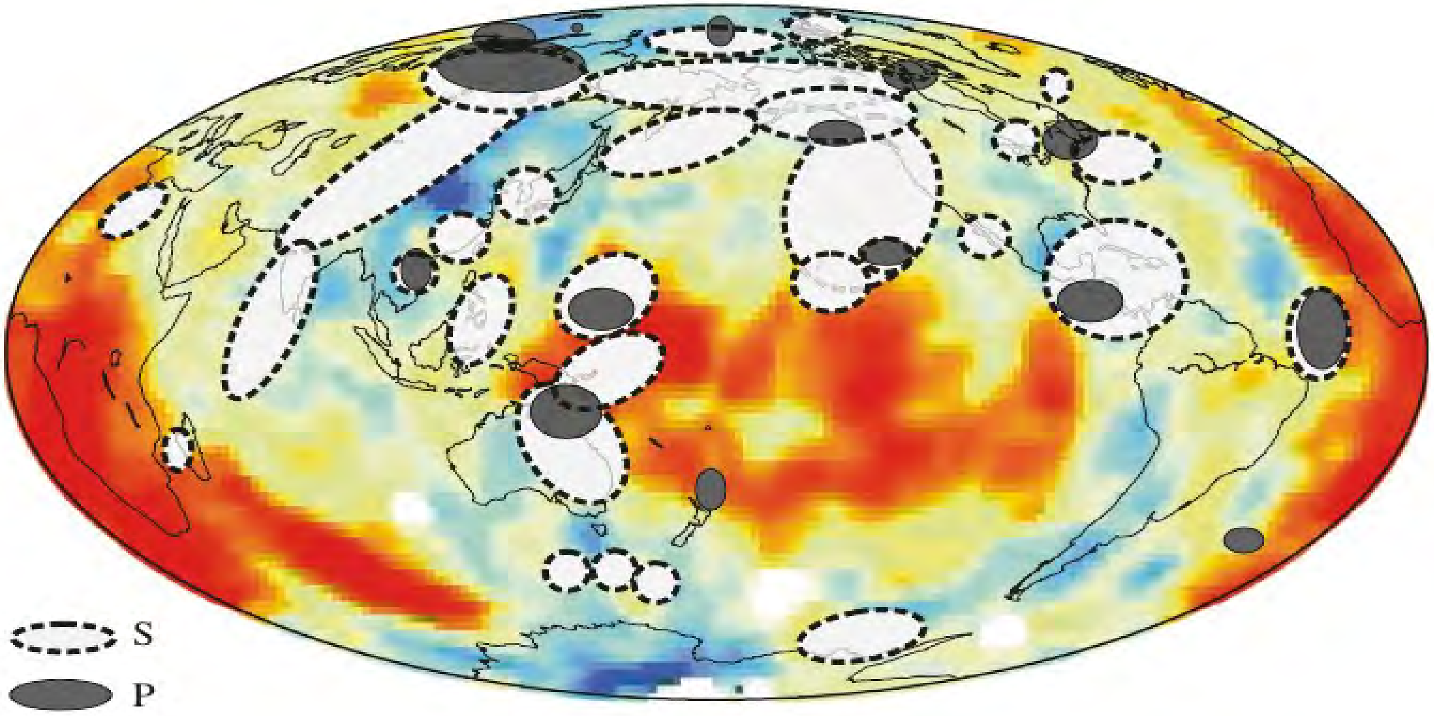

Locations of observations of D" reflections overlaid on the tomography model of Grand, 2002.

Cobden et al, 2015

Seismic phase change mapping

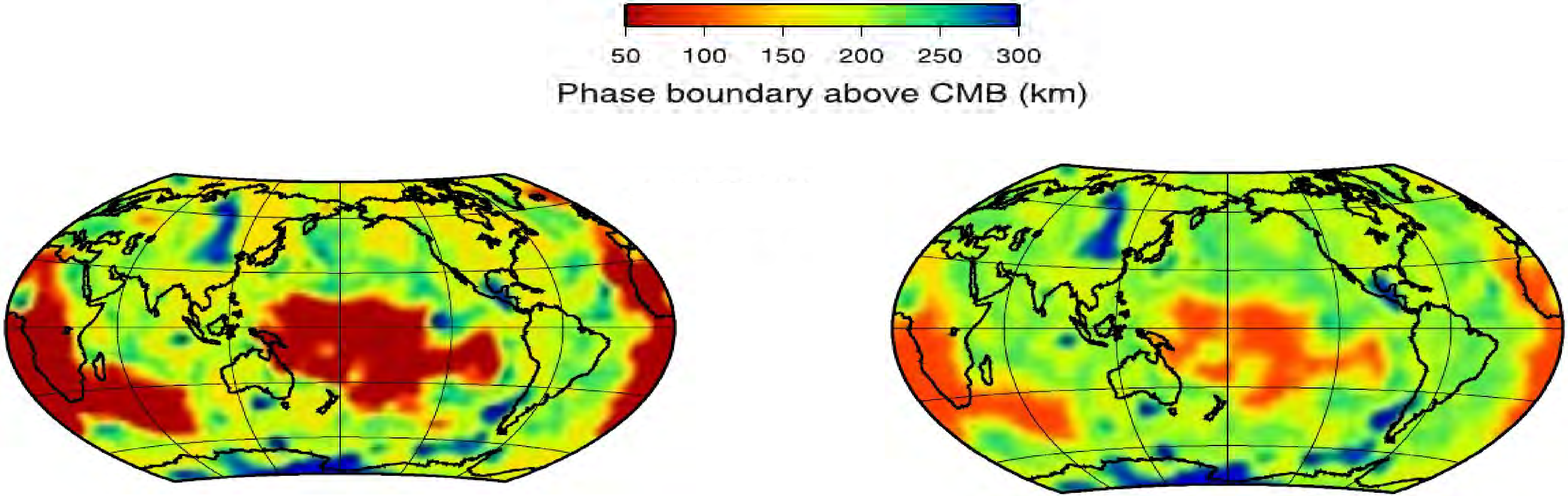

γ = 12 MPa/K

γ = 6 MPa/K

Lower mantle tomography and phase change mapping

Daoyuan Sun[1] and Don Helmberger[1]

JOURNAL OF GEOPHYSICAL RESEARCH, VOL. 113, B10305, doi: 10.1029/2007JB005289, 2008

Université de Lille

Pv to pPv transition in the mantle ?

Mineralogical effects on the detectability of the postperovskite boundary

Brent Grocholski[a,1], Krystle Catalli[a], Sang-Heon Shim[a], and Vitali Prakapenka[b]

PNAS | **February 14, 2012** | vol. 109 | no. 7 | **2277**

Experimental evidence for perovskite and post-perovskite coexistence throughout the whole D″ region

Denis Andrault [a,*], Manuel Muñoz [b], Nathalie Bolfan-Casanova [a], Nicolas Guignot [c], Jean-Philippe Perrillat [d], Giuliana Aquilanti [d], Sakura Pascarelli [d]

D. Andrault et al. / Earth and Planetary Science Letters 293 (2010) 90–96

Thickness and Clapeyron slope of the post-perovskite boundary

Krystle Catalli[1], Sang-Heon Shim[1] & Vitali Prakapenka[2]

NATURE | Vol 462 | 10 December 2009

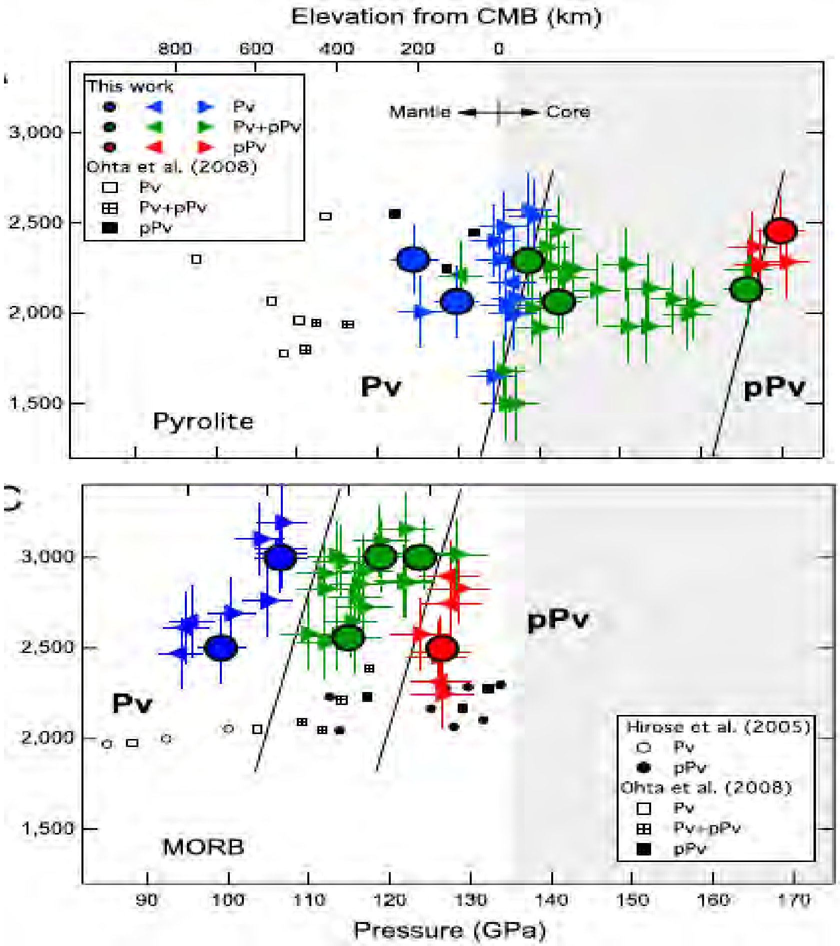

Transformation kinetics between Pv and pPv

Laser-heated DAC

Starting material: Enstatite, 14% Fe

Pressure medium: Argon

Conversion to Pv at ~90 GPa

Conversion to pPv at various P and T

Continuous monitoring with XRD

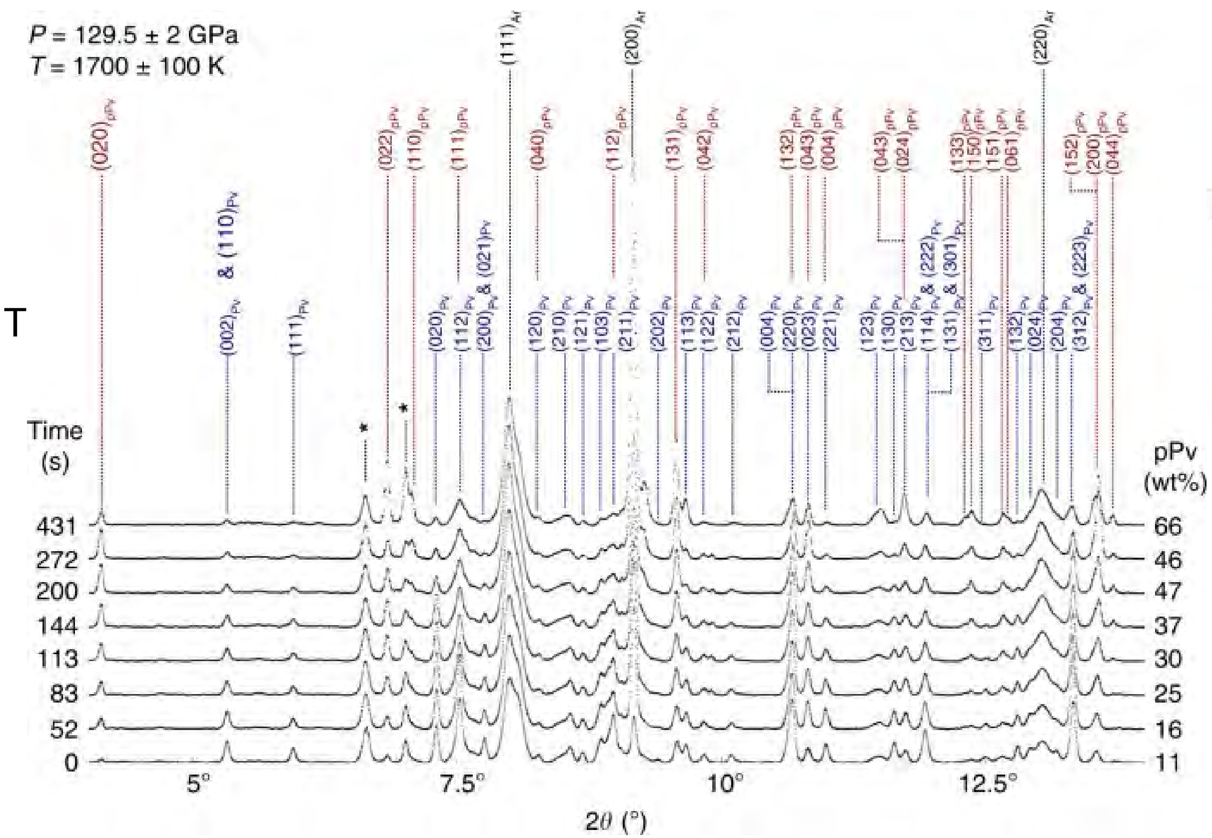

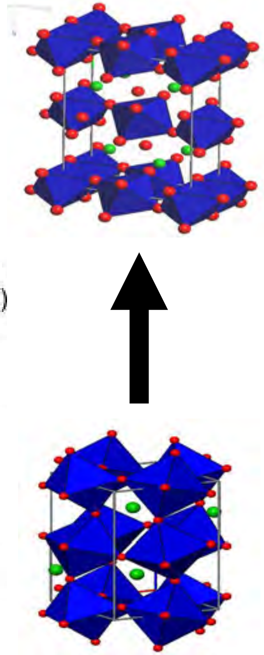

PETRA III
P02.2

Langrand et al *Nat Comm* **10**, 5680 (2019).

Transformation kinetics
Experimental model

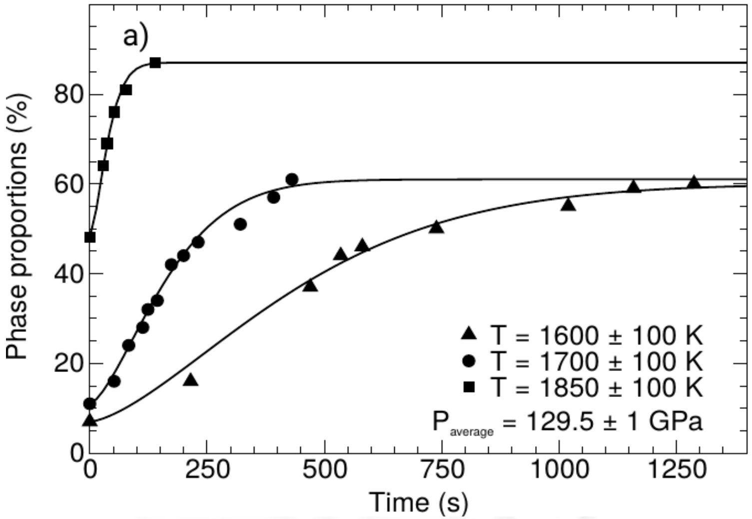

$$\xi(t) = 1 - e^{-\left(\frac{t}{\tau}\right)^n}$$

τ: transformation time scale

Langrand et al *Nat Comm* **10**, 5680 (2019).

Transformation kinetics
Experimental model

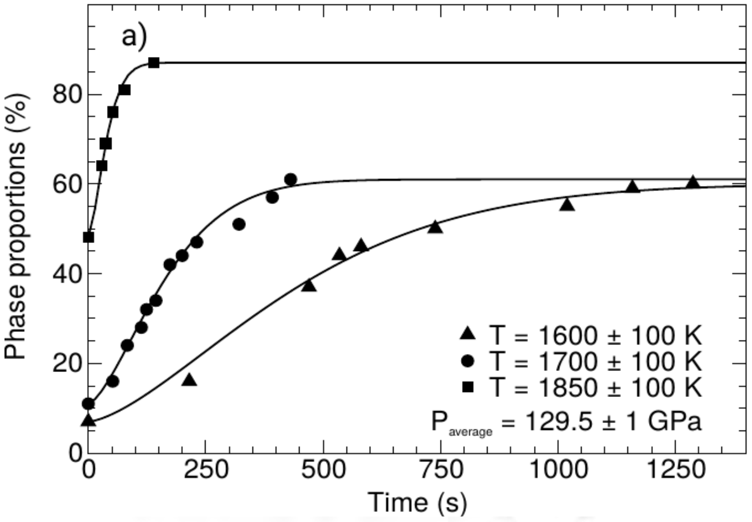

$$\xi(t) = 1 - e^{-\left(\frac{t}{\tau}\right)^n}$$

τ: transformation time scale

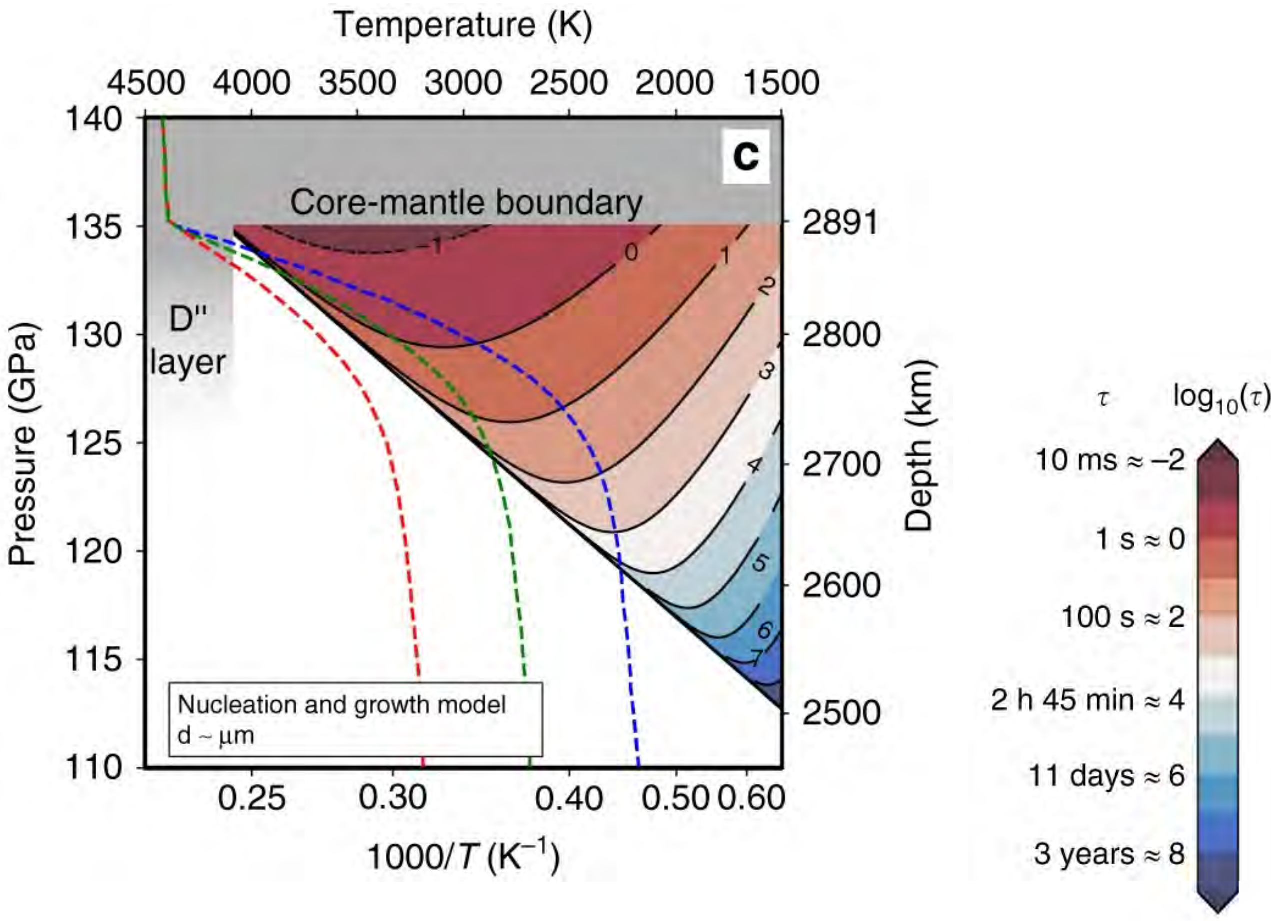

Langrand et al *Nat Comm* **10**, 5680 (2019).

Transformation kinetics
Effect of grain size ?

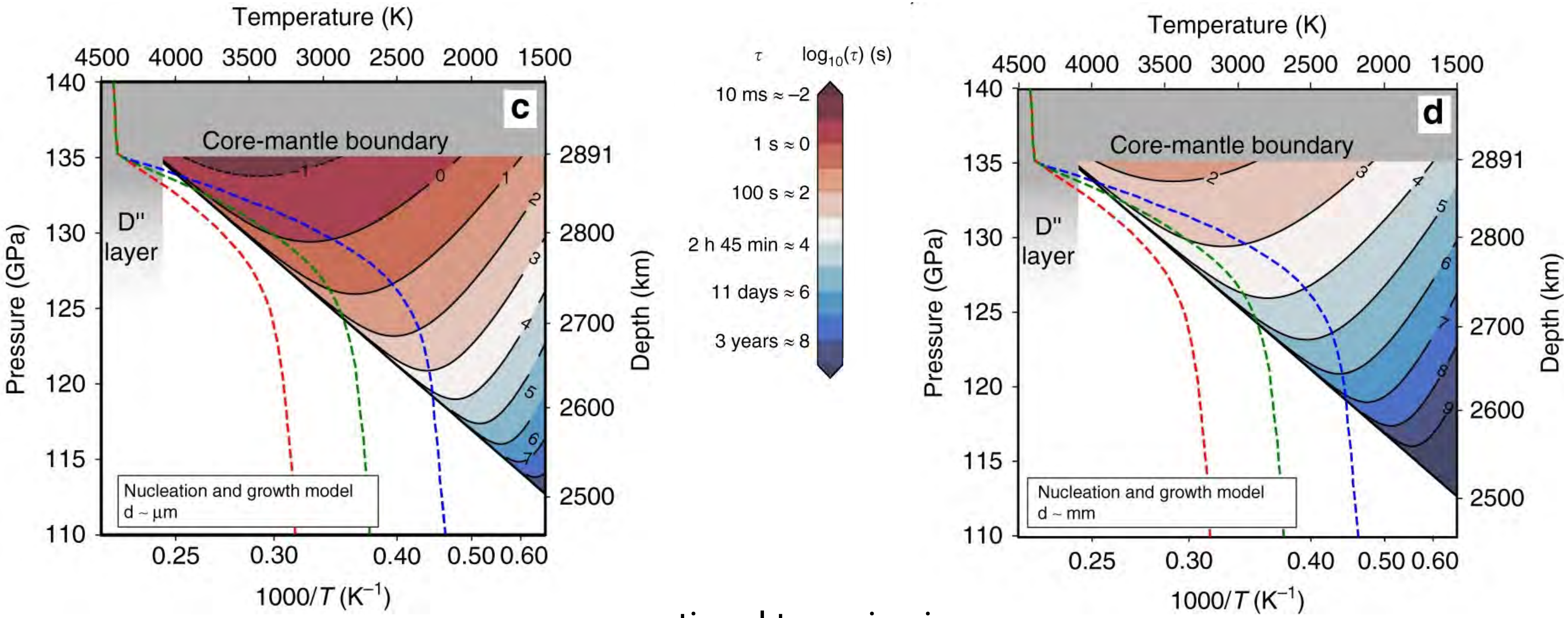

τ: proportional to grain size

Constant product growth rate hypothesis for nucleation and growth model

No effect of grain size in a shear transformation model

Pv – pPv transformation
Seismic detectability

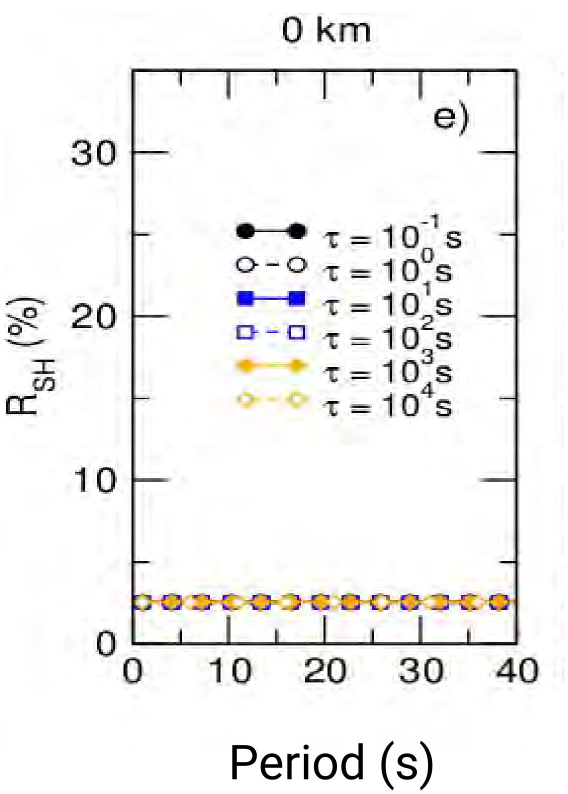

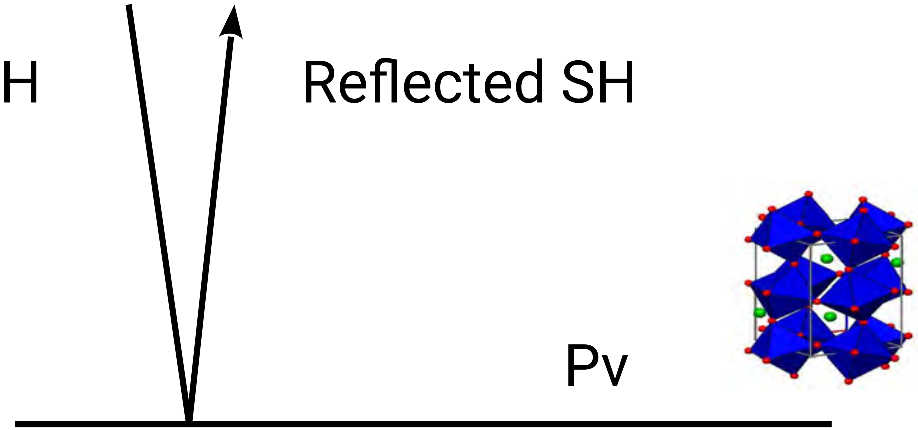

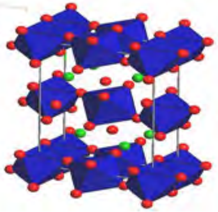

- SH wave
- Vertical incidence
- Infinitely thin interface

R_{SH} = 2.5%

Independant of kinetics
Independant of wave period

Langrand et al *Nat Comm* **10**, 5680 (2019).

Pv – pPv transformation
Seismic detectability

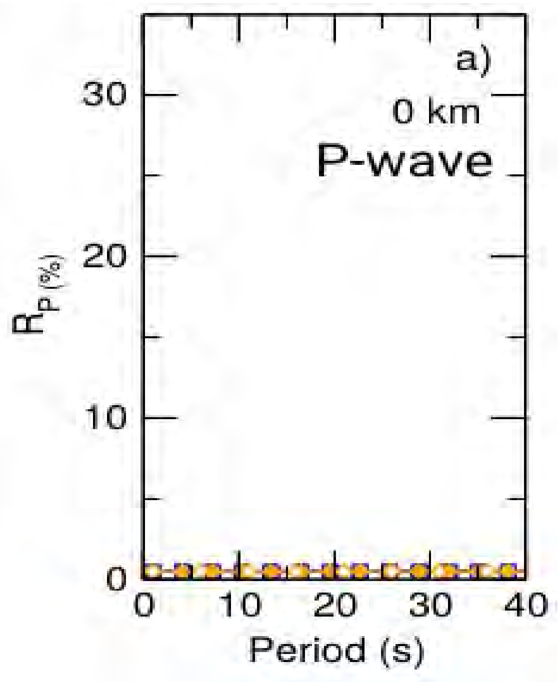

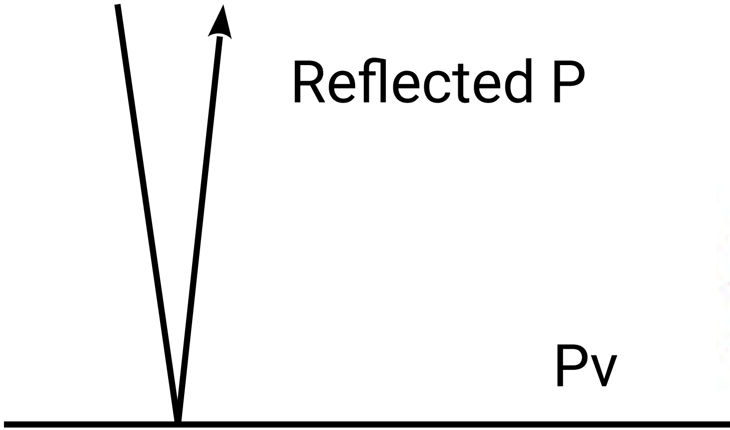

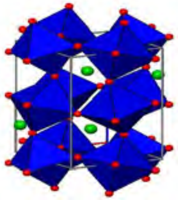

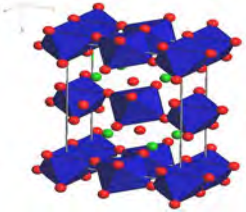

- P wave
- Vertical incidence
- Infinitely thin interface

R_{SH} = 0.5 %

Independant of kinetics
Independant of wave period

Langrand et al *Nat Comm* **10**, 5680 (2019).

Effect of kinetics and phase coexistence loop

Seismic attenuation in a phase change coexistence loop

Yanick Ricard *, J. Matas, F. Chambat
Laboratoire des Sciences de la Terre, CNRS, Université de Lyon, Bat Géode, 2 rue Raphael Dubois, 69622, Villeurbanne, 07, France

Physics of the Earth and Planetary Interiors 176 (2009) 124–131

Constraining the kinetics of mantle phase changes with seismic data

S. Durand, F. Chambat, J. Matas and Y. Ricard
Laboratoire de Sciences de la Terre, CNRS UMR5570, École Normale Supérieure de Lyon, Université de Lyon, Université Claude Bernard Lyon 1, 46 Allée d'Italie, 69364 Lyon Cedex 07, France. E-mail: stephanie.durand@ens-lyon.fr

Geophys. J. Int. (2012) **189**, 1557–1564

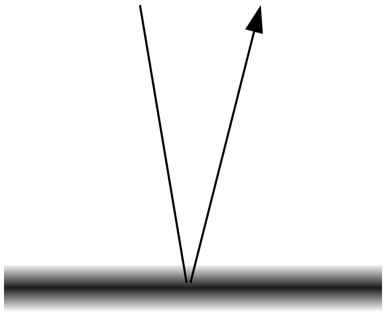

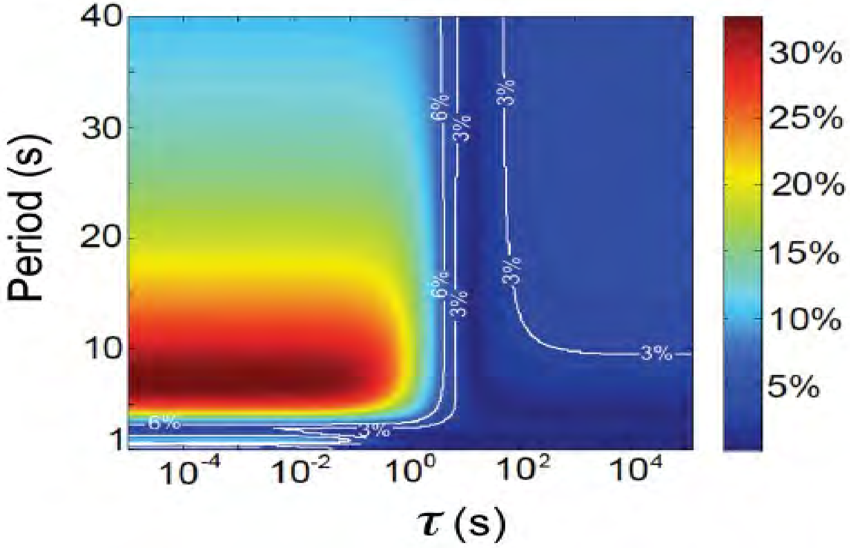

Reflection coefficient at 410 km
vertically incident SH wave
10 km thick olivine-wadsleyite loop
Horizontal axis: transformation kinetics
Vertical axis: wave period

Pv – pPv transformation with kinetics
Seismic detectability – SH wave

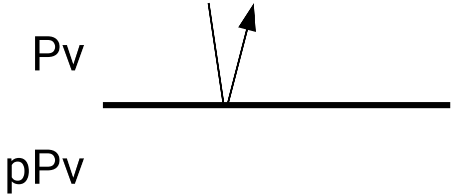

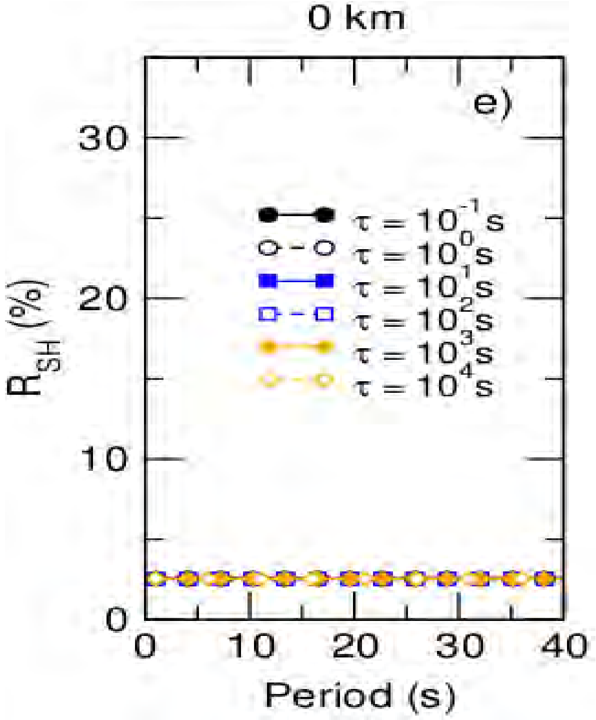

Langrand et al *Nat Comm* **10**, 5680 (2019).

Pv – pPv transformation with kinetics
Seismic detectability – SH wave

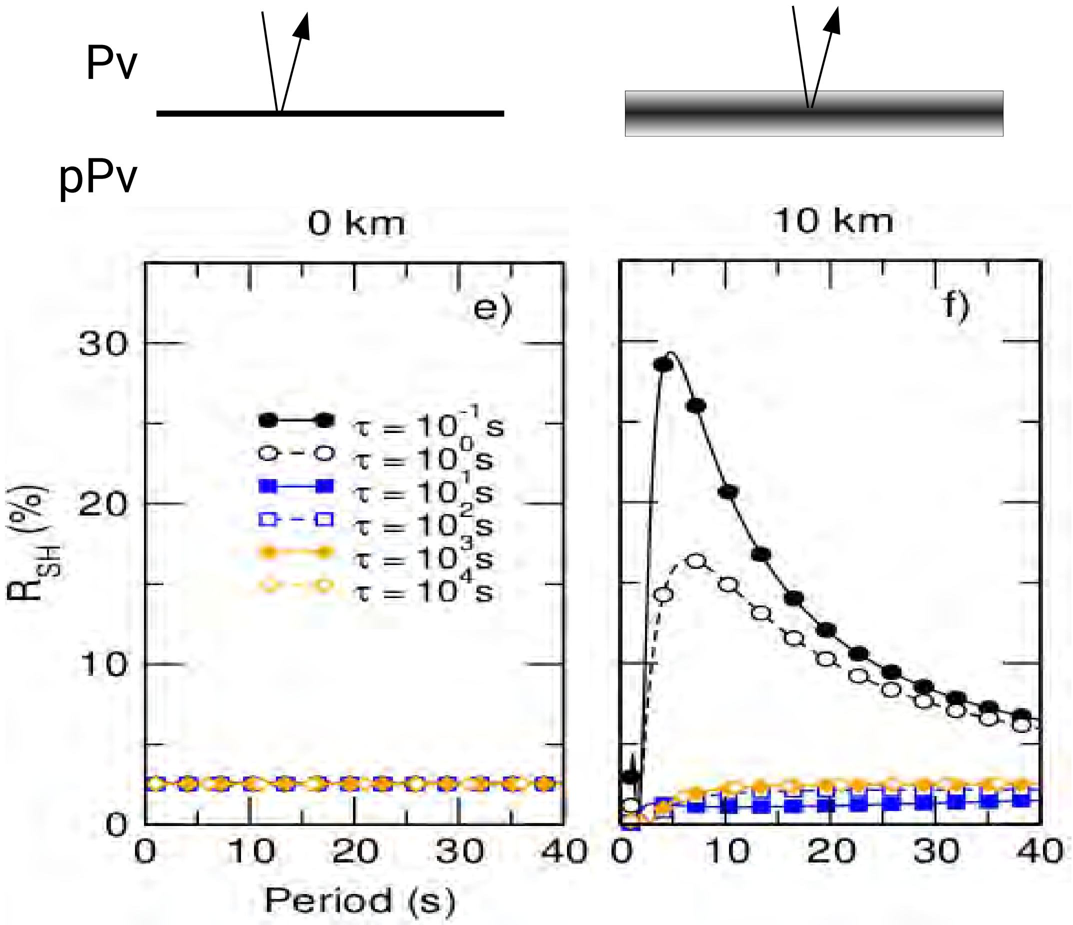

Langrand et al *Nat Comm* **10**, 5680 (2019).

Pv – pPv transformation with kinetics
Seismic detectability – SH wave

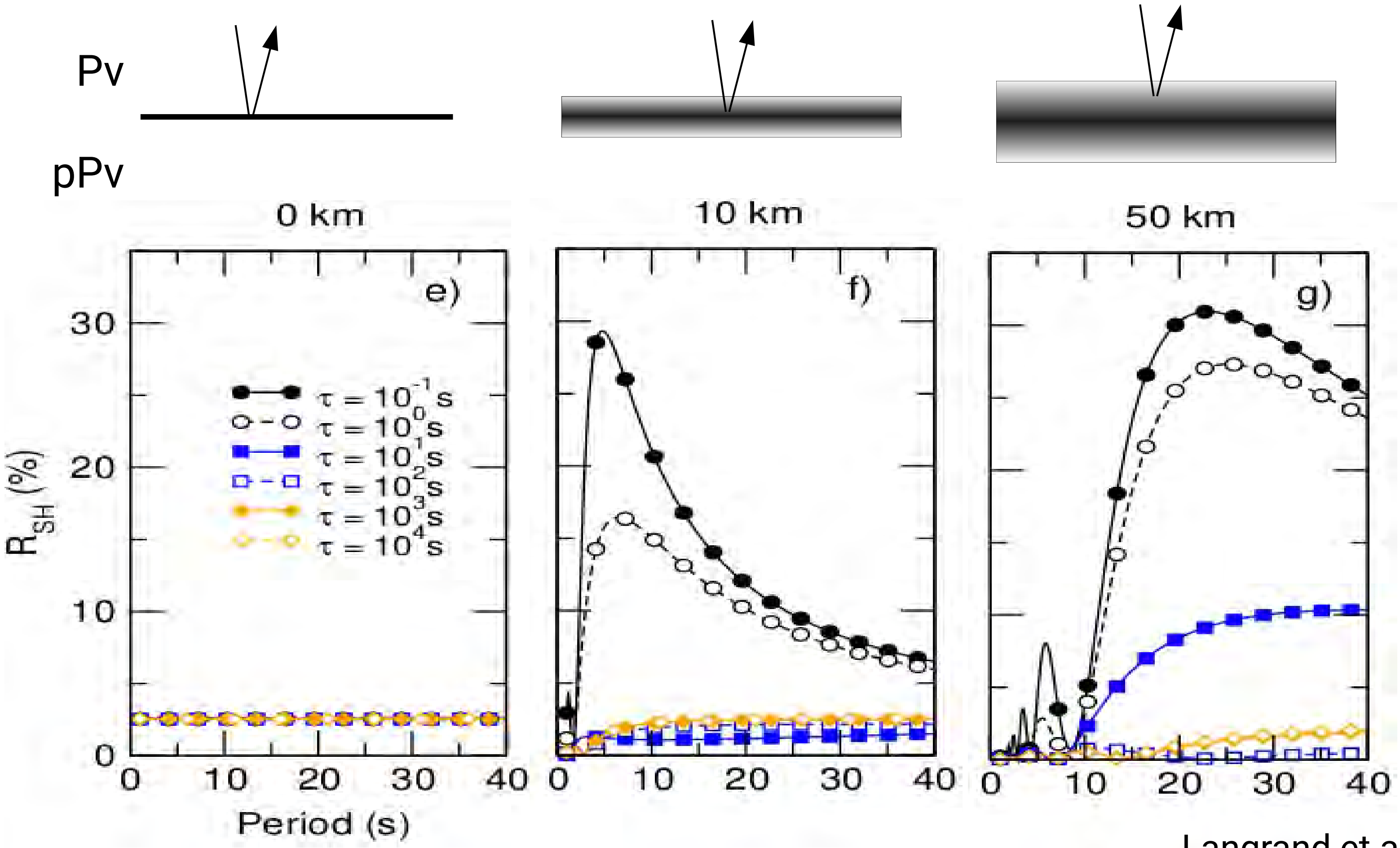

Langrand et al *Nat Comm* **10**, 5680 (2019).

Pv – pPv transformation with kinetics
Seismic detectability – SH wave

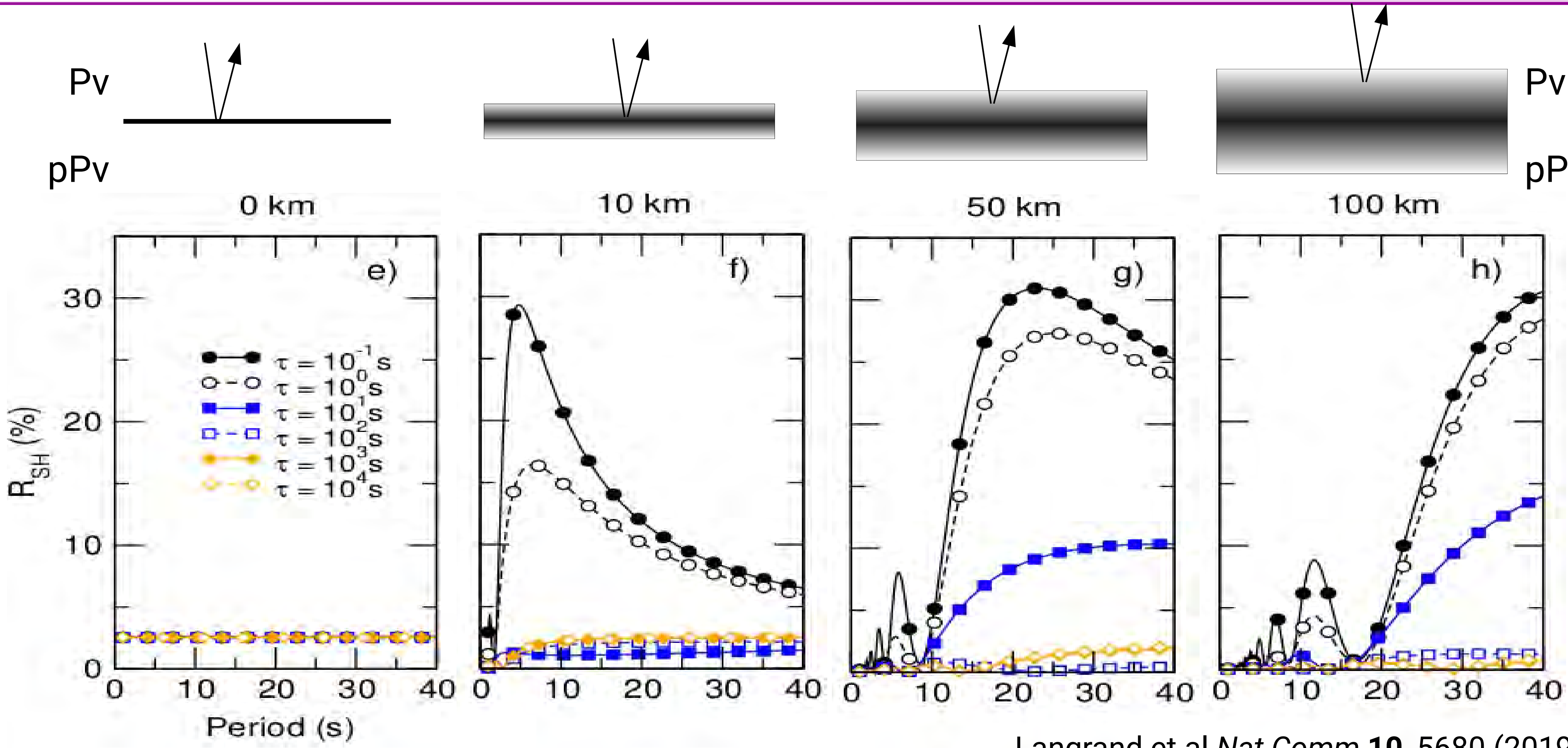

Langrand et al *Nat Comm* **10**, 5680 (2019).

Pv – pPv transformation with kinetics
Seismic detectability – P wave

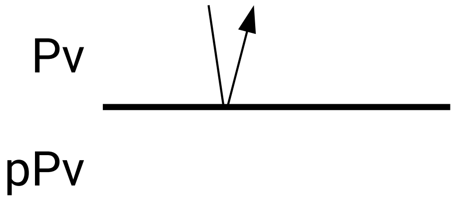

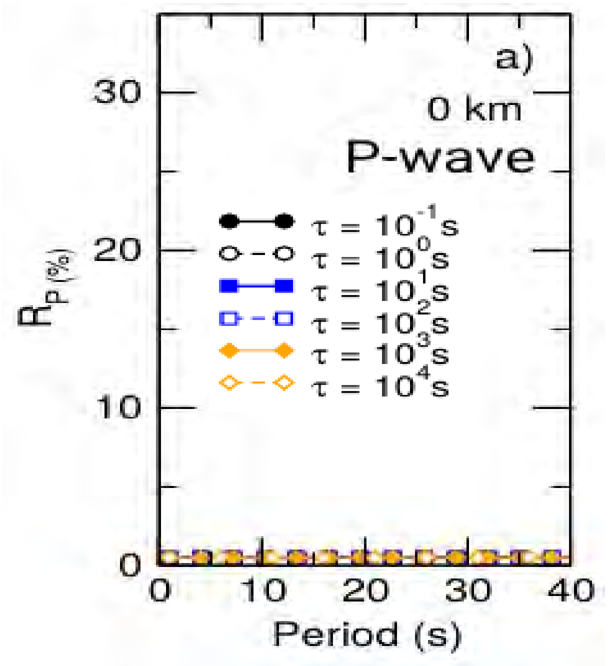

Langrand et al *Nat Comm* **10**, 5680 (2019).

Pv – pPv transformation with kinetics
Seismic detectability – P wave

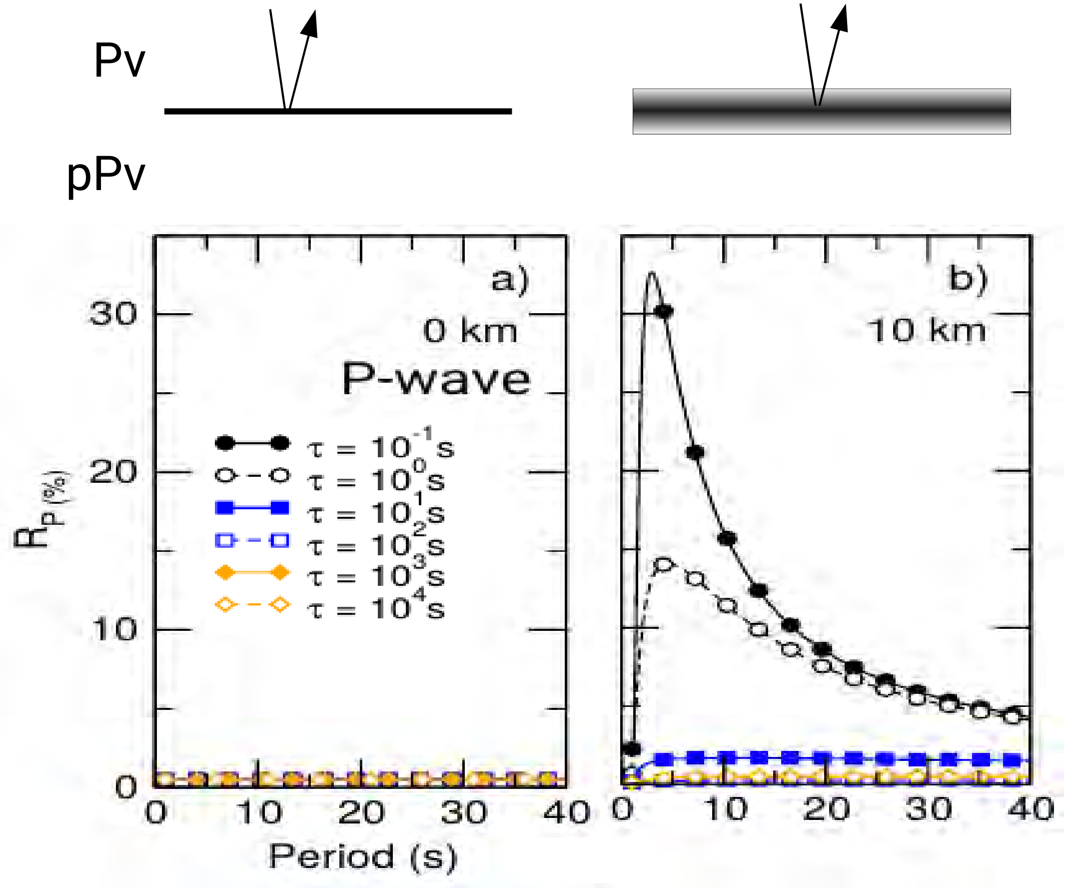

Langrand et al *Nat Comm* **10**, 5680 (2019).

Pv – pPv transformation with kinetics
Seismic detectability – P wave

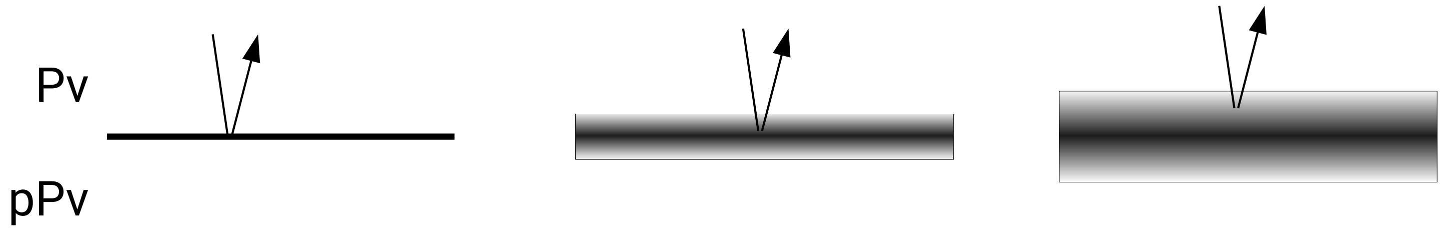

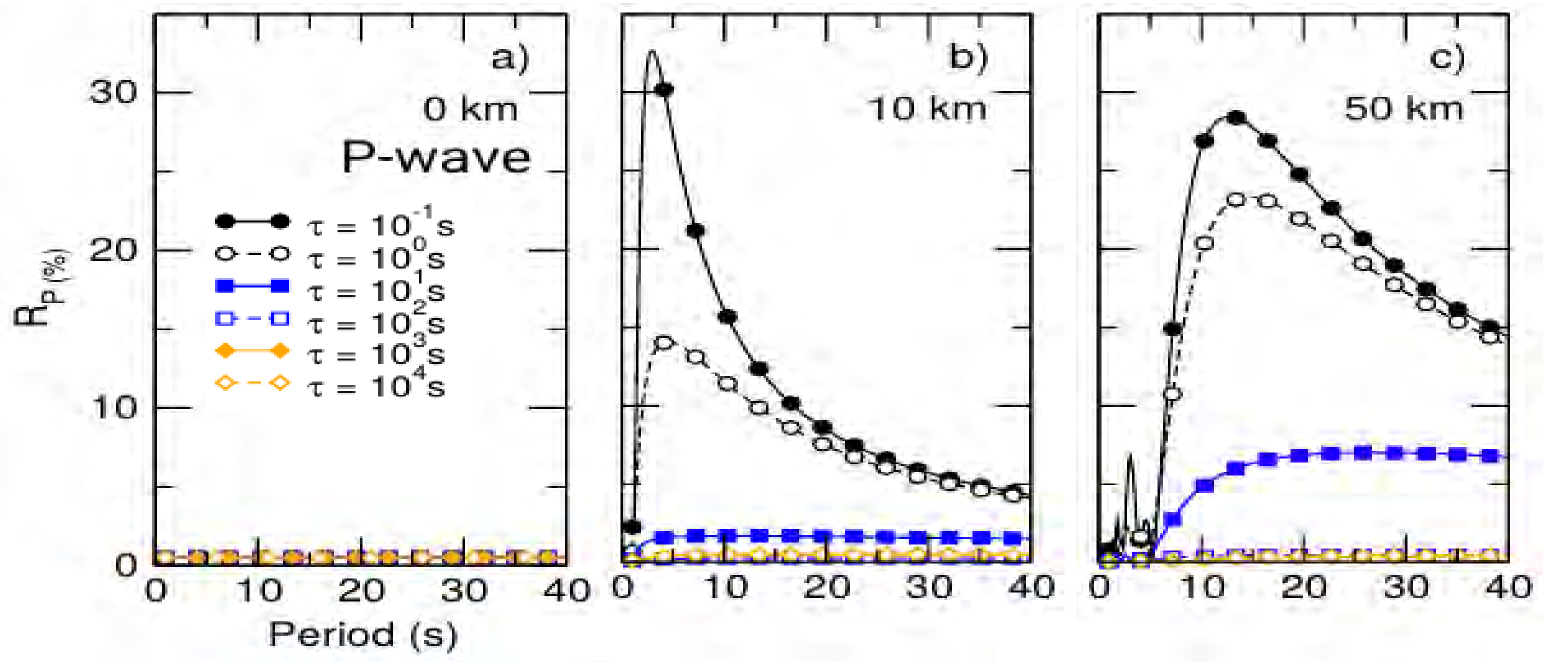

Langrand et al *Nat Comm* **10**, 5680 (2019).

Pv – pPv transformation with kinetics
Seismic detectability – P wave

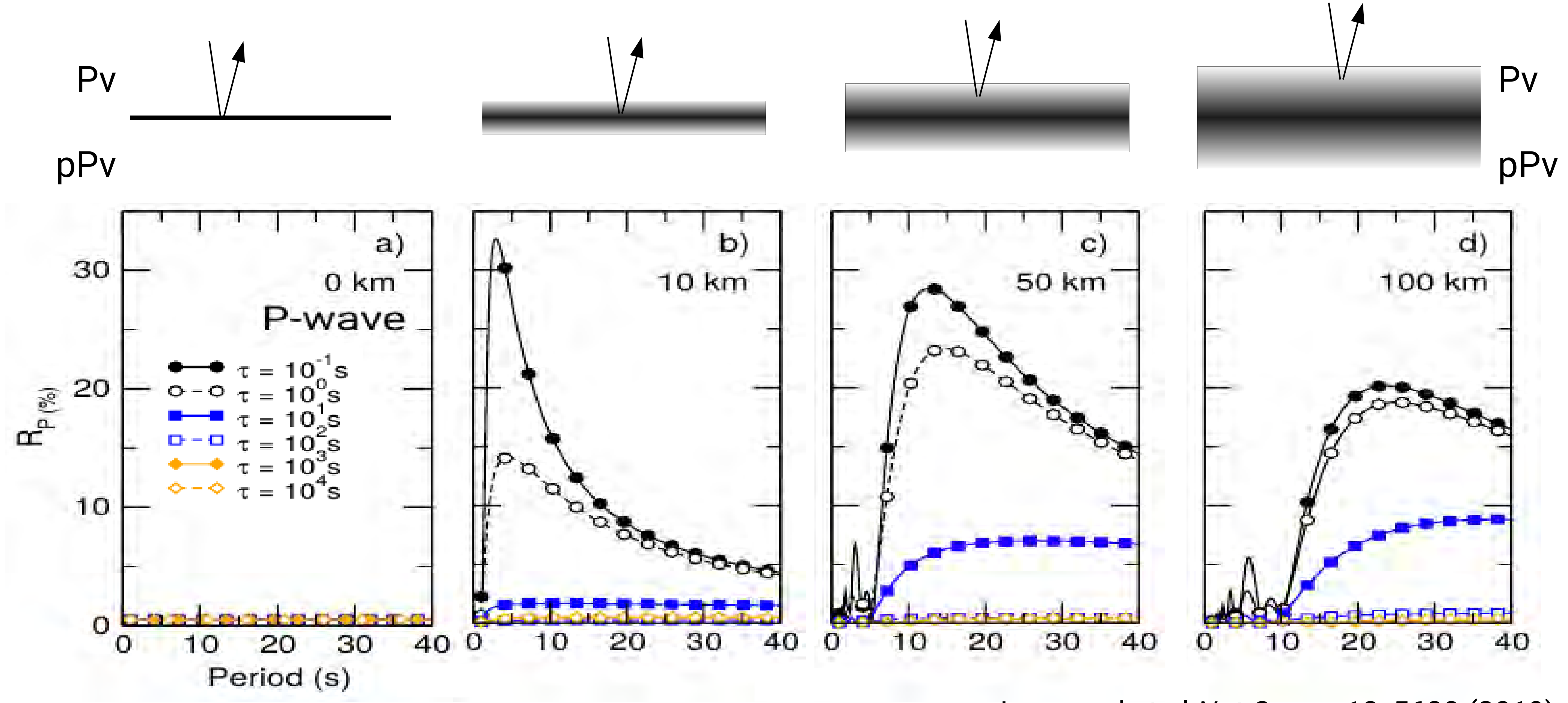

Langrand et al *Nat Comm* **10**, 5680 (2019).

On the detectability of the Pv-pPv transformation

Kinetics of Pv / pPv transformation

Pure Pv

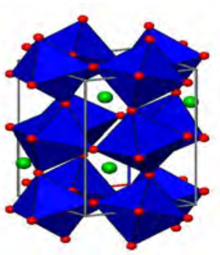

Pure pPv

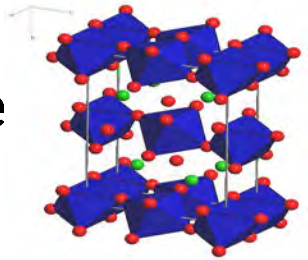

Kinetics of Pv / pPv transformation

Fast at D" pressure and temperature conditions

- Experimental (grains ~ 1 µm): 10^{-1} à 10^{3} s,
- Extrapolation (shear model): no grain size effect
- Extrapolation (nucleation and growth model, grains ~ 1 mm): 10^{2} à 10^{6} s (11 days)

Pure Pv

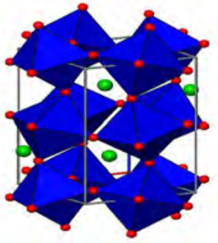

Pure pPv

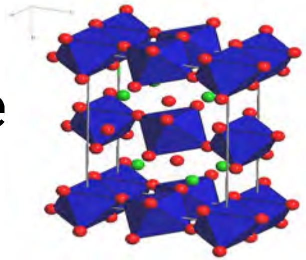

Université de Lille

Kinetics of Pv / pPv transformation

Fast at D” pressure and temperature conditions

- Experimental (grains ~ 1 µm): 10^{-1} à 10^{3} s,
- Extrapolation (shear model): no grain size effect
- Extrapolation (nucleation and growth model, grains ~ 1 mm): 10^{2} à 10^{6} s (11 days)

Seismic detectability

- Refection amplification due to
  - Transformation kinetics
  - Pv / pPv coexistence loop
- Efficient for thick Pv / pPv coexistence layer (up to 100 km)
- Depends on wave period

Pure Pv

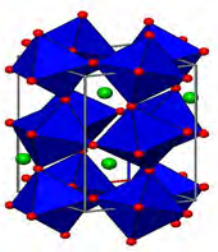

Pure pPv

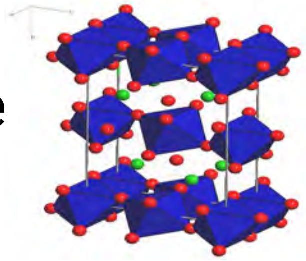

Kinetics of Pv / pPv transformation

Fast at D” pressure and temperature conditions

- Experimental (grains ~ 1 µm): 10^{-1} à 10^{3} s,
- Extrapolation (shear model): no grain size effect
- Extrapolation (nucleation and growth model, grains ~ 1 mm): 10^{2} à 10^{6} s (11 days)

Seismic detectability

- Refection amplification due to
  - Transformation kinetics
  - Pv / pPv coexistence loop
- Efficient for thick Pv / pPv coexistence layer (up to 100 km)
- Depends on wave period

Potential

- Cut-off frequency : thickness of Pv / pPv coexistence layer
- Amplitude measurements : kinetics of phase transformation
  → temperature / grain size

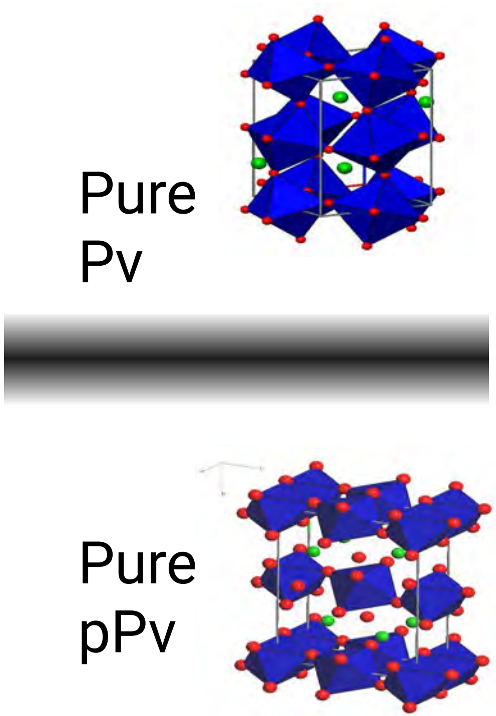

Microstructures

Transformation Mechanism?

Strong inheritance of texture between perovskite and post-perovskite in the D″ layer

David P. Dobson[1,2]★, Nobuyoshi Miyajima[3], Fabrizio Nestola[4], Matteo Alvaro[4], Nicola Casati[5], Christian Liebske[2], Ian G. Wood[1] and Andrew M. Walker[6]

NATURE GEOSCIENCE | VOL 6 | JULY 2013

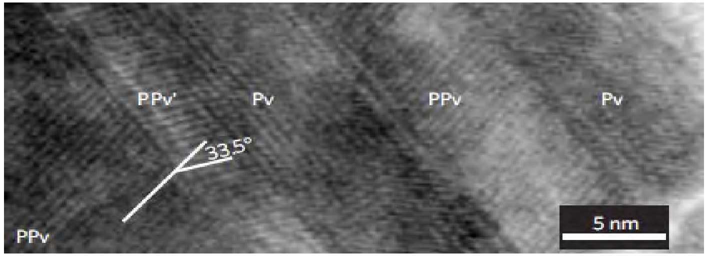

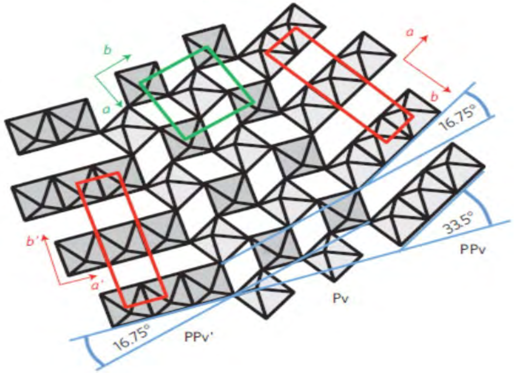

Transformation Mechanism?

Strong inheritance of texture between perovskite and post-perovskite in the D″ layer

David P. Dobson[1,2]*, Nobuyoshi Miyajima[3], Fabrizio Nestola[4], Matteo Alvaro[4], Nicola Casati[5], Christian Liebske[2], Ian G. Wood[1] and Andrew M. Walker[6]

NATURE GEOSCIENCE | VOL 6 | JULY 2013

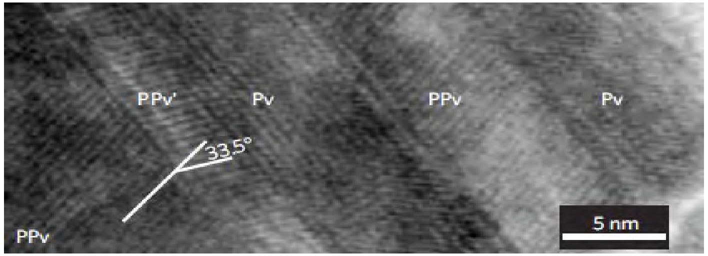

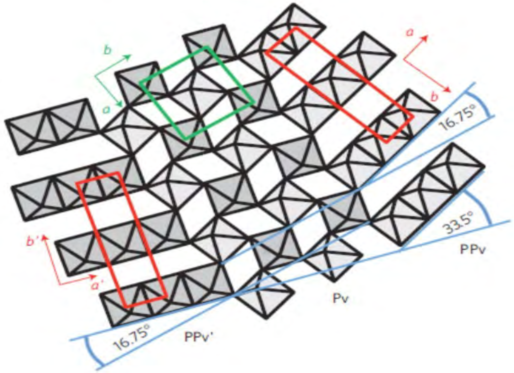

If martensitic (with orientation relationships):

- Texture memory
- Deformation history preserved
- Anisotropy

If no orientation relationships

- Loss of memory
- Random texture
- Loss of anisotropy

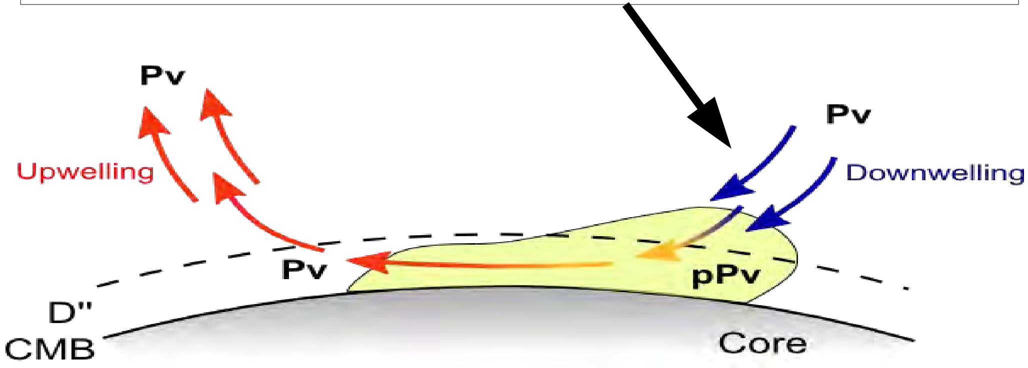

Pv / pPv Coherent Mechanisms

Tsuchiya et al, 2004

simulations $MgSiO_3$

Pv

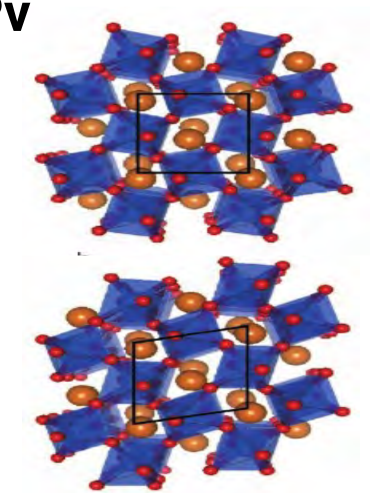

pPv

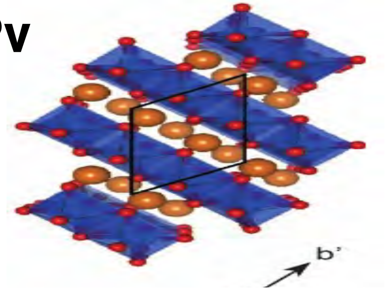

Tsuchiya et al, 2004

simulations $MgSiO_3$

Pv

pPv

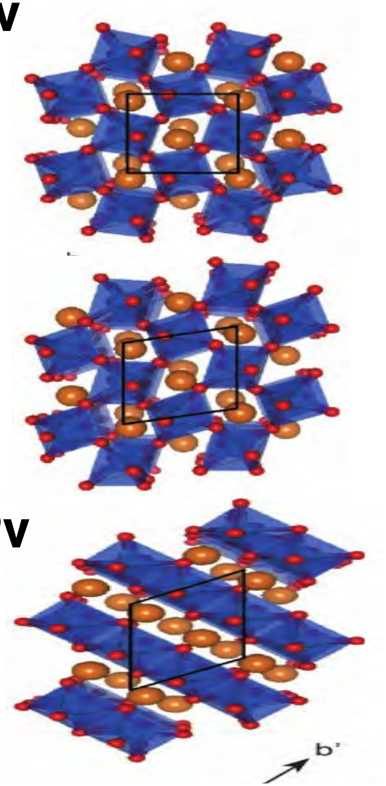

Oganov et al, 2005

simulations $MgSiO_3$

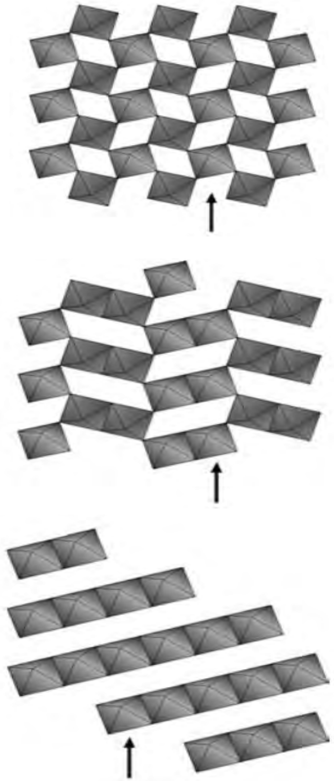

Université de Lille

Pv / pPv Coherent Mechanisms

Tsuchiya et al, 2004
simulations $MgSiO_3$

Pv

pPv

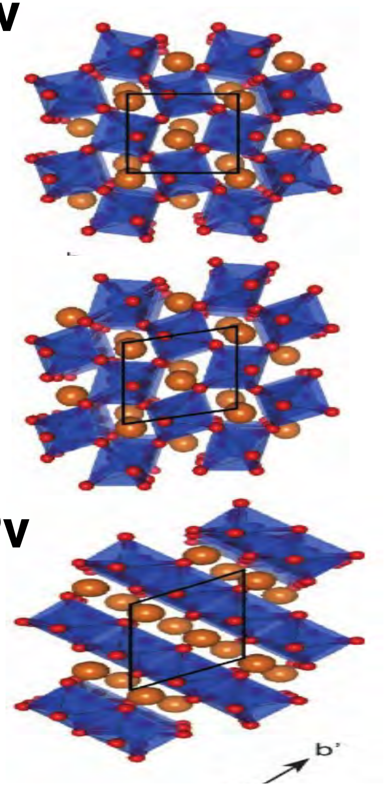

Oganov et al, 2005
simulations $MgSiO_3$

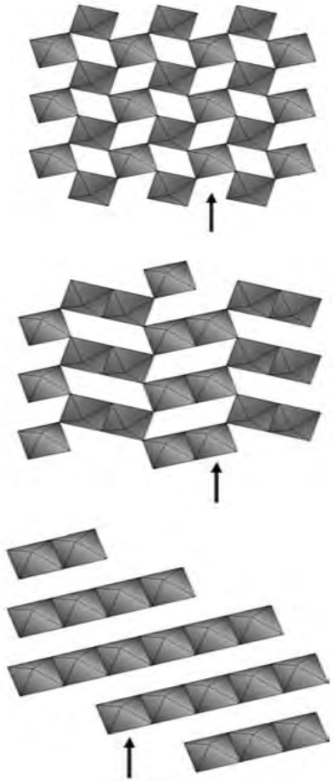

Dobson et al, 2013
TEM + experiments $NaNiF_3$

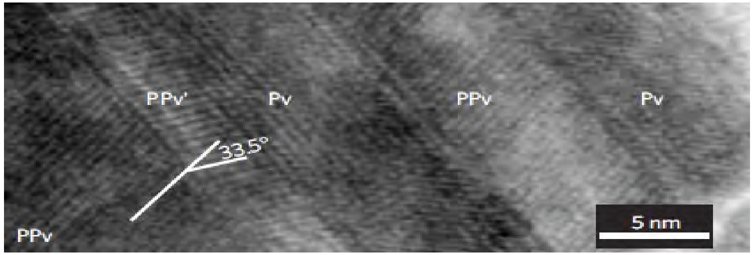

Green: perovskite
Red: post-perovskite

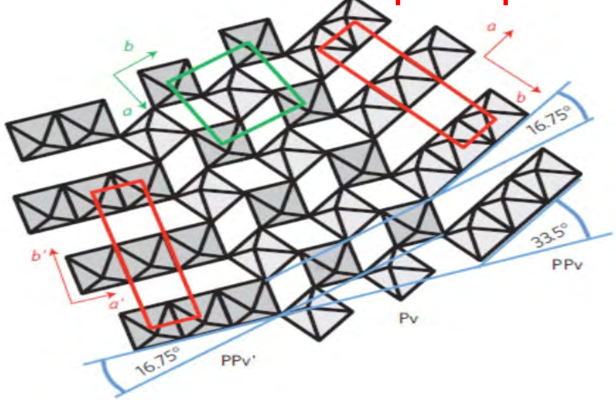

Pv / pPv Coherent Mechanisms

Tsuchiya et al, 2004
simulations $MgSiO_3$

Pv

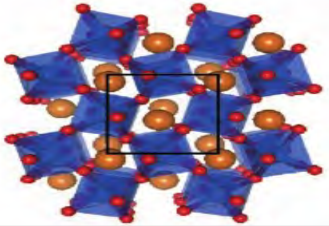

~45°
rotation
around c-axis

pPv

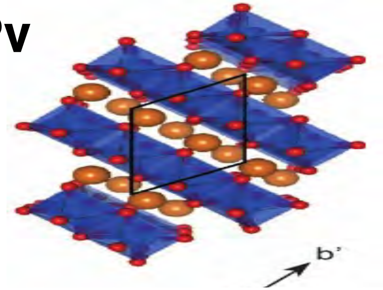

Oganov et al, 2005
simulations $MgSiO_3$

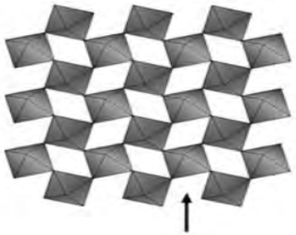

random
rotation
around c-axis

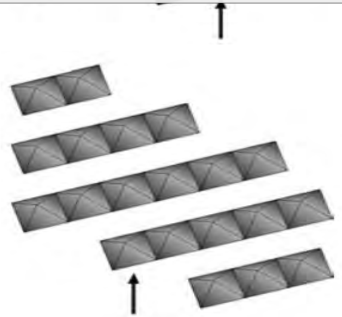

Dobson et al, 2013
TEM + experiments $NaNiF_3$

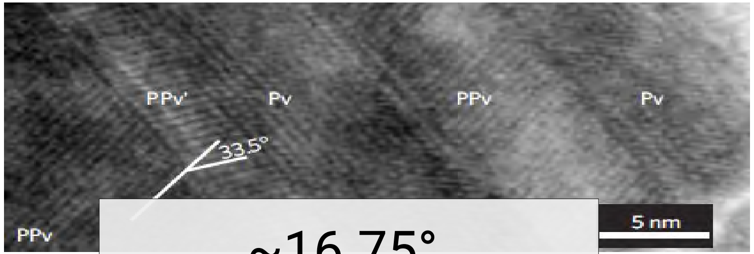

~16.75°
rotation
around c-axis

Green: perovskite
Red: post-perovskite

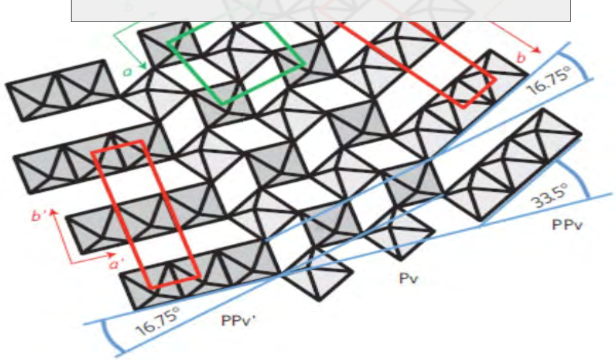

Multigrain Crystallography

Diamond anvil cell sitting on a rotation stage

Collect images at every rotation step

Typical numbers

- Rotation range: $\Delta\omega = 45°$
- Rotation step: $\delta\omega = 0.5°$
- 90 diffraction images per P/T point

Allows to map orientations of individual grains inside a diamond anvil cell, at mantle P/T conditions.

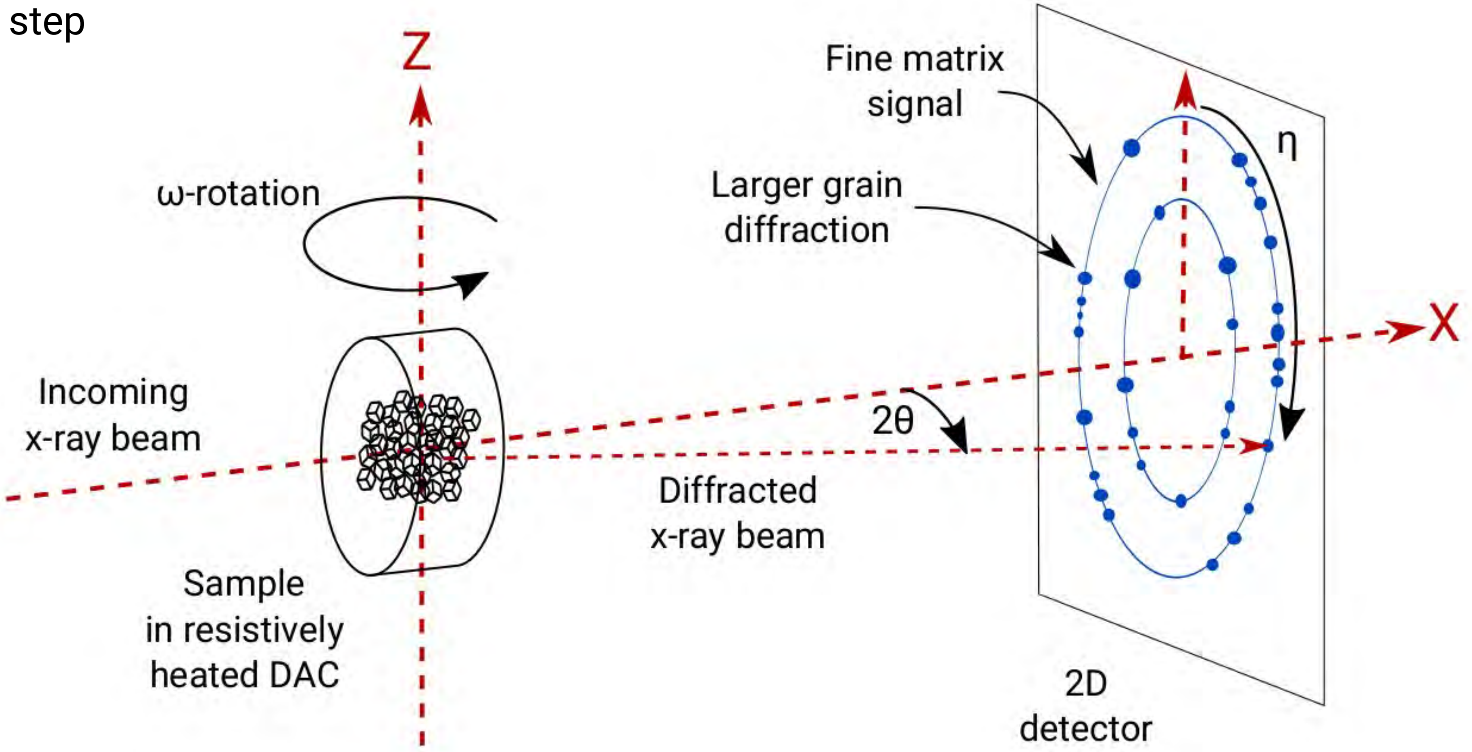

Nisr *et al*, *High Pres. Res.* 2014

Multigrain XRD: Capabilities

Typical numbers

- ~10^4 spots per P/T point
- Random walk through orientation space to identify grains
- ~ 10^6 iterations
- ~ 5.10^2 to 5.10^3 indexed grains per P/T point

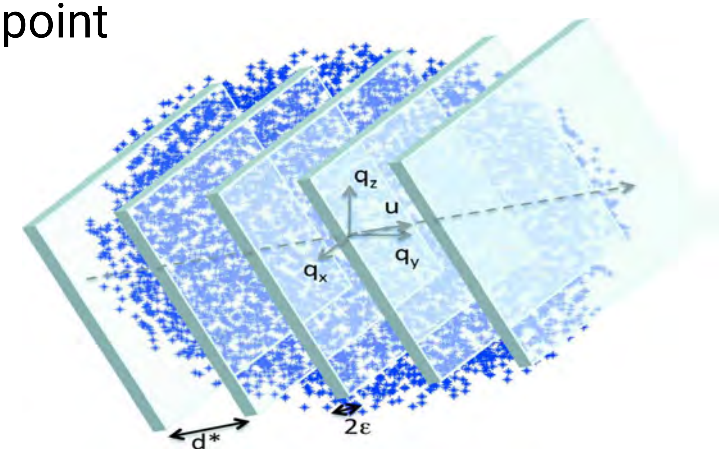

Ilustration:
Wejdemanna and Poulsen, *J. Appl. Cryst*. 2016

Results

Average sample

- Fine matrix vs. grains volume ratio
- Phase proportions

Grain scale, for each indexed grain

- Orientation
- Relative volume

Potential for deep Earth Mineralogy

- Follow mineral microstructures at deep Earth mantle pressure ***AND*** temperatures

Nisr *et al*, *J. Geoph Res*. 2012
Nisr *et al*, *High Pres. Res*. 2014
Rosa *et al*, *J. Appl. Cryst*. 2015
Rosa *et al*, *J. Geoph Res*. 2016
Langrand *et al*, *J. Appl. Cryst*. 2017

Pv – pPv transformation in $NaCoF_3$

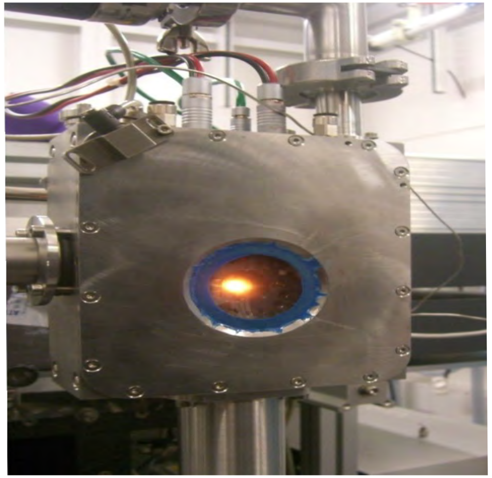

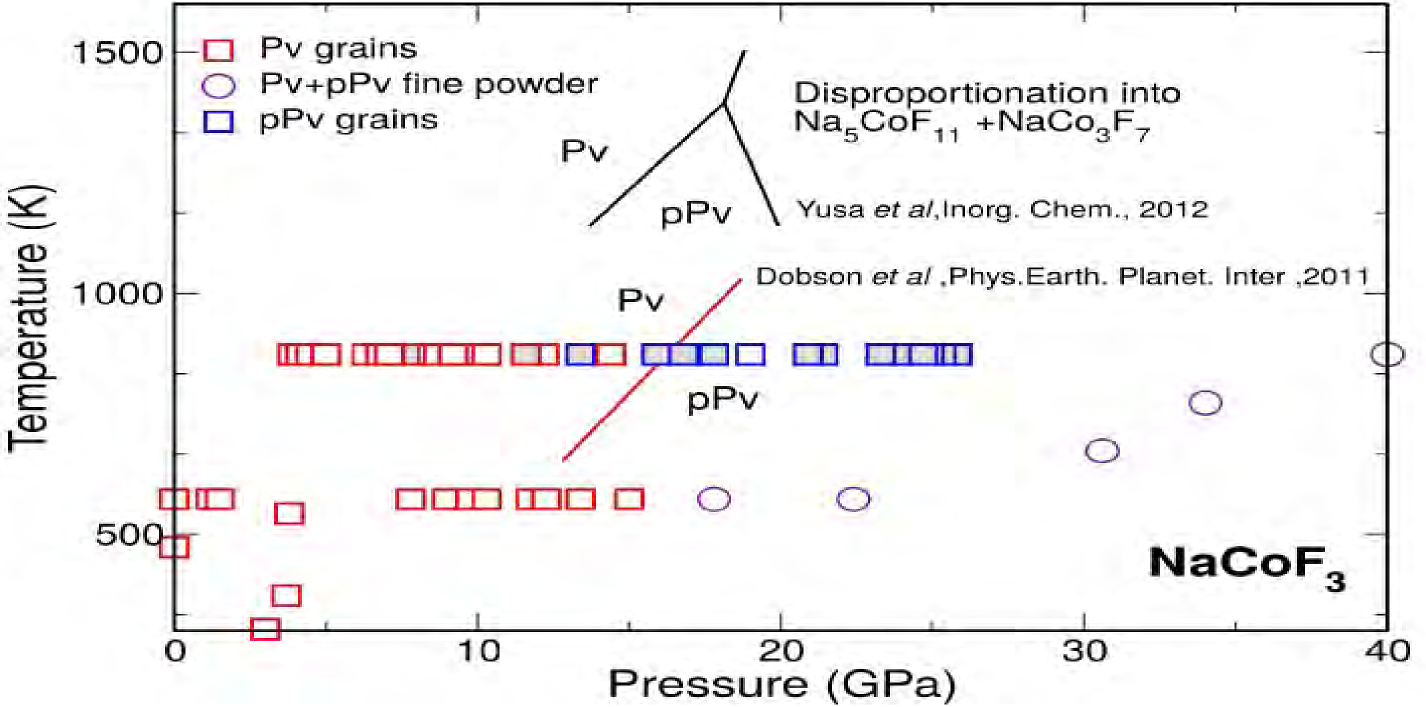

Sample

- $NaCoF_3$
- Pv to pPv transition at ~15 GPa

Confinement

- Resistive heating DAC
- Rhenium gasket
- Run duration: ~10s of hours for each T

ID 27

Pv to pPv, 900 K

$NaCoF_3$ Perovskite

Before Transformation

P = 14.1 GPa – T = 900 K

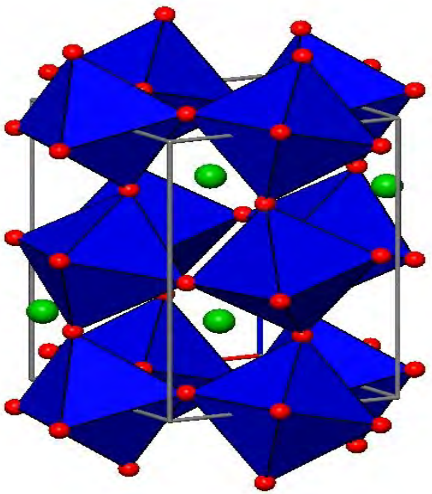

$NaCoF_3$ post-Perovskite

After Transformation

P = 17.5 GPa – T = 900 K

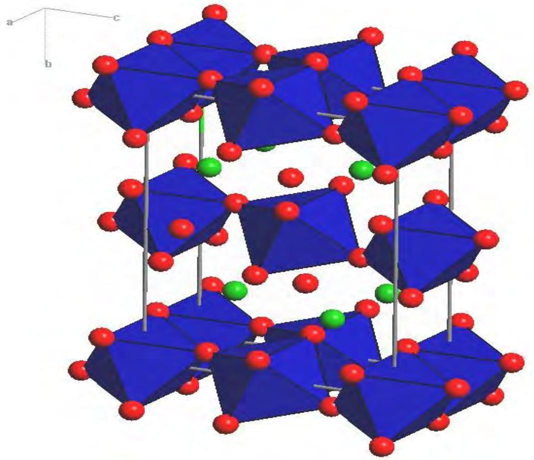

Merkel *et al*, in prep.

$NaCoF_3$ Perovskite

Before Transformation

P = 14.1 GPa – T = 900 K

Fine matrix: 47 %
Extracted spots: 62232
Indexed spots: 61 %
Indexed grains: 1028

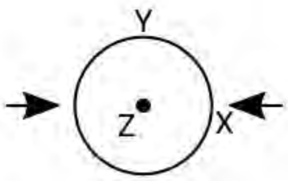

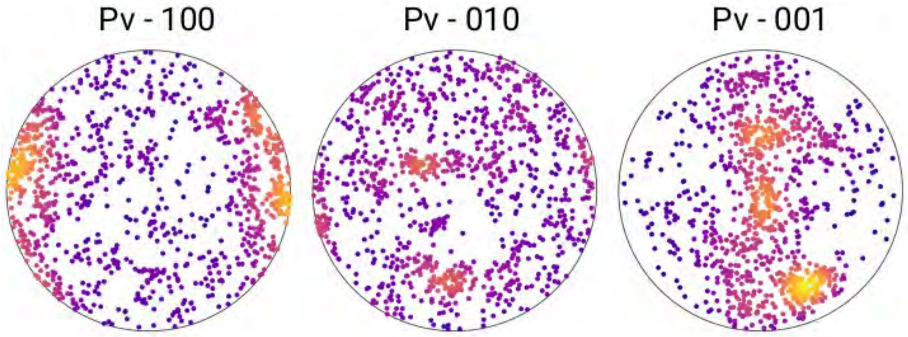

Indexed Pv grains

Pv to pPv, 900 K – Grain Orientations

$NaCoF_3$ Perovskite

Before Transformation

P = 14.1 GPa – T = 900 K

Fine matrix:	47 %
Extracted spots:	62232
Indexed spots:	61 %
Indexed grains:	1028

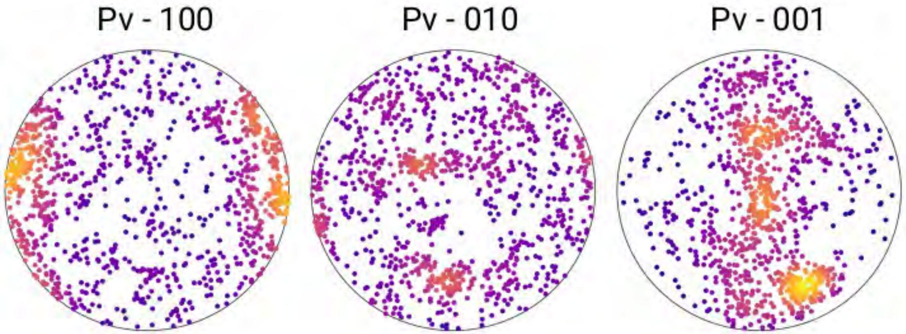

Indexed Pv grains

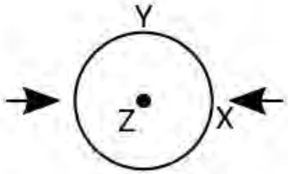

$NaCoF_3$ post-Perovskite

After Transformation

P = 17.5 GPa – T = 900 K

Fine matrix:	22 %
Extracted spots :	121293
Indexed spots:	77 %
Indexed grains:	2946

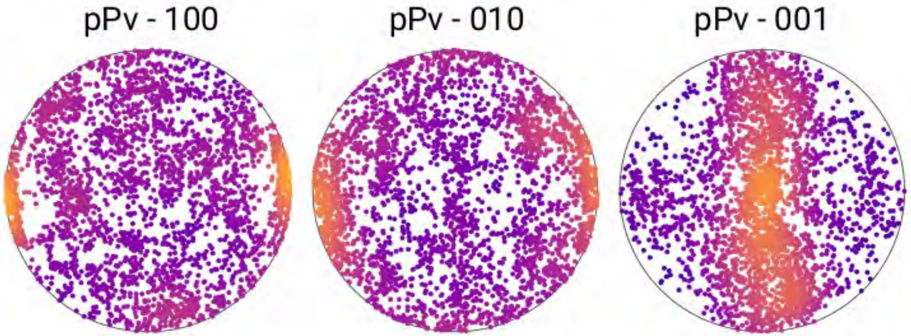

Indexed pPv grains

Experiment

START

Pv, experimental
1028 grains orientations

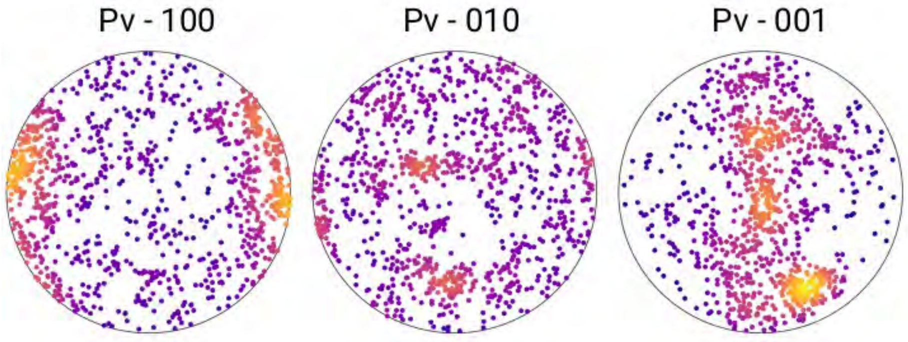

END

pPv, experimental
2946 grain orientations

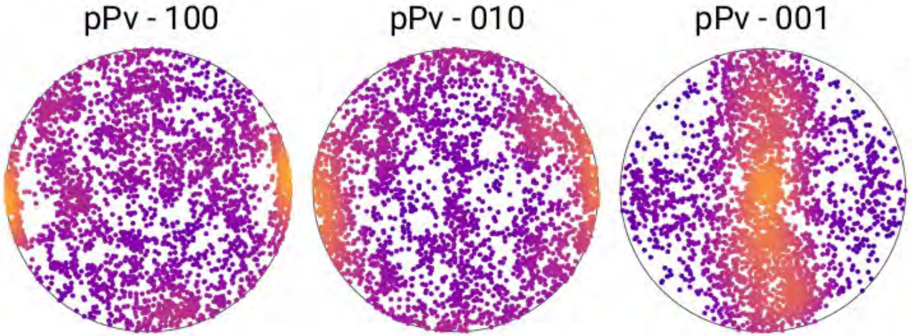

Number of grains multiplied by 3
Fine matrix: 47% to 22%

Orientation concentrations for $(001)_{Pv}$
~ Orient conc for $(001)_{pPv}$

Orientation concentrations for $(100)_{Pv}$
~ Orient conc for $(010)_{pPv}$

In favor of a Dobson-like mechannism

Merkel *et al*, in prep.

Experiment

START

Pv, experimental
1028 grains orientations

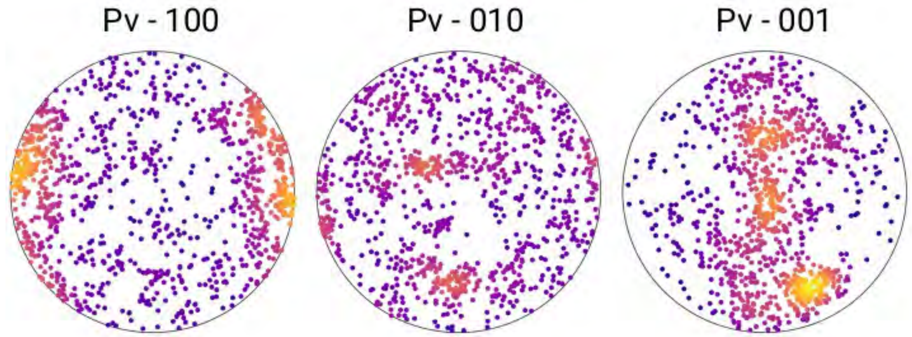

END

pPv, experimental
2946 grain orientations

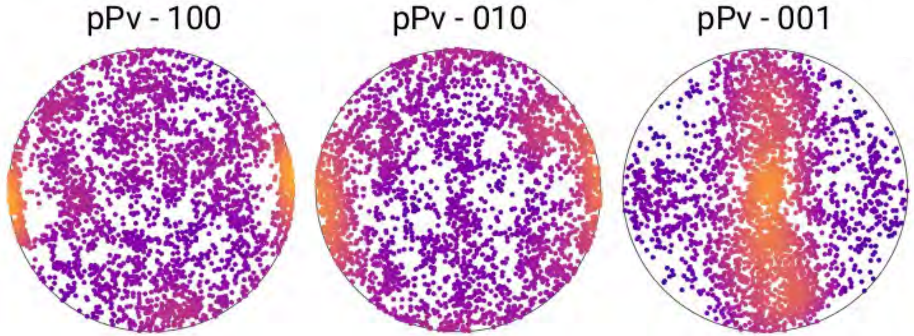

Simulation

pPv, Dobson orientation relationships
2056 grain orientations

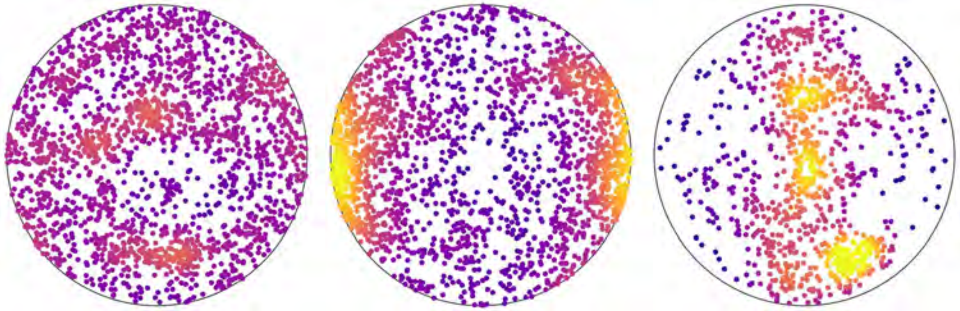

Experiment

START

Pv, experimental
1028 grains orientations

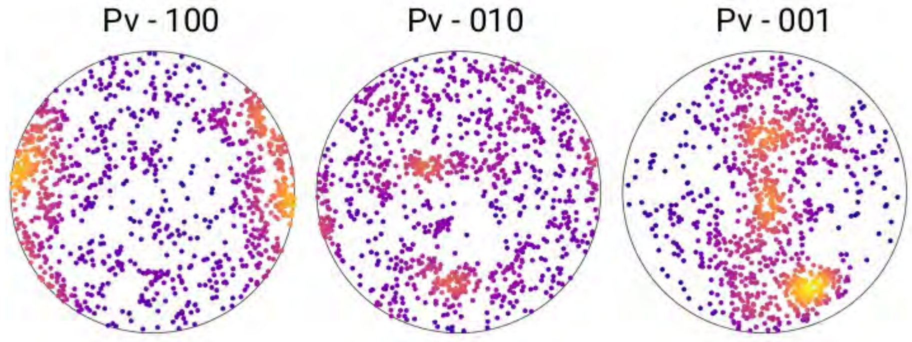

END

pPv, experimental
2946 grain orientations

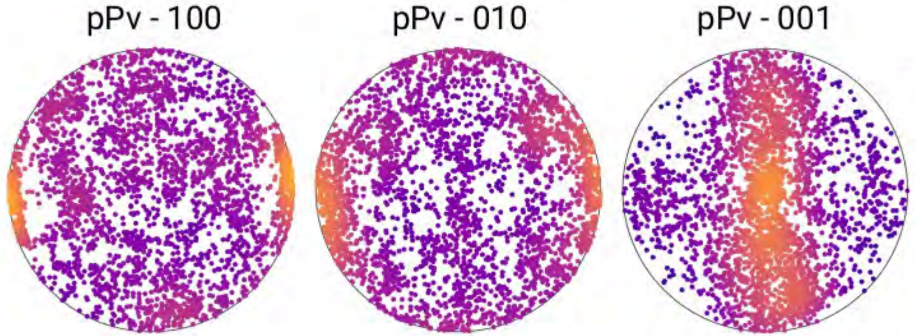

Simulation

pPv, Dobson orientation relationships
2056 grain orientations

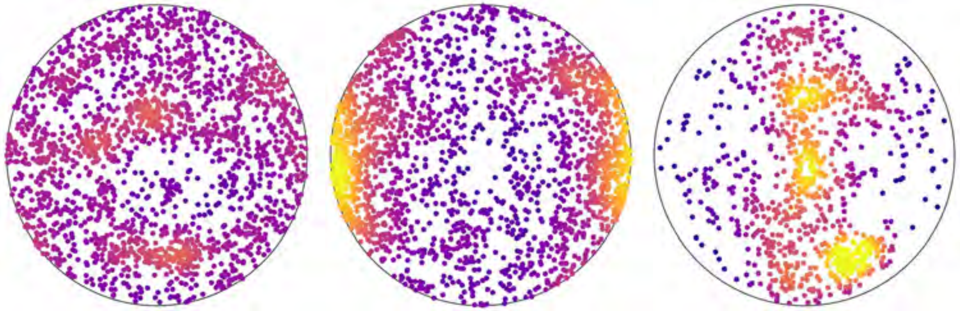

Add random nucleation for the missing 900 grains

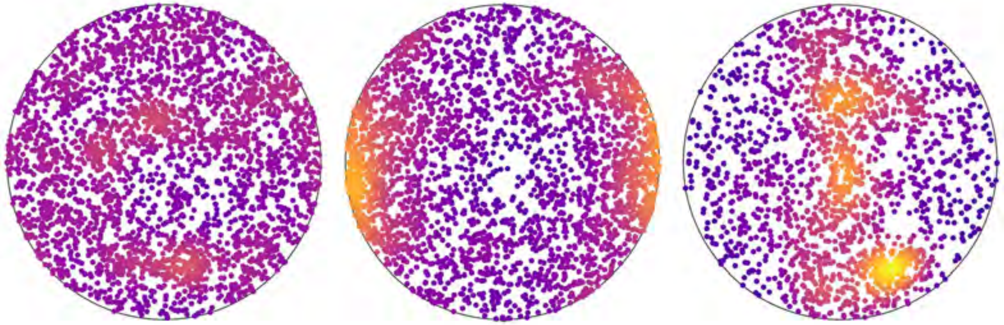

pPv to Pv, 900 K

$NaCoF_3$ post-perovskite

Before Transformation

P = 17.8 GPa – T = 900 K

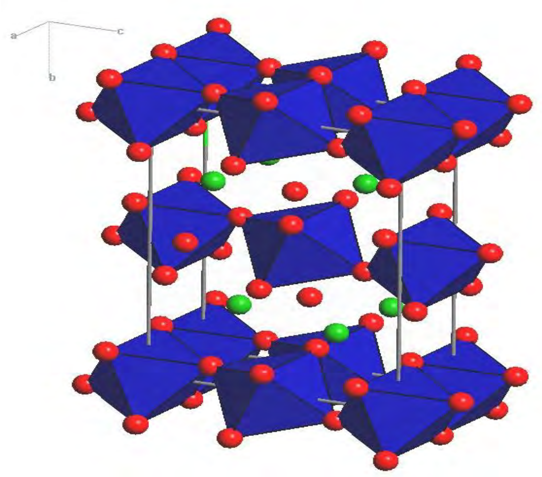

$NaCoF_3$ Perovskite

After Transformation

P = 13.4 GPa – T = 900 K

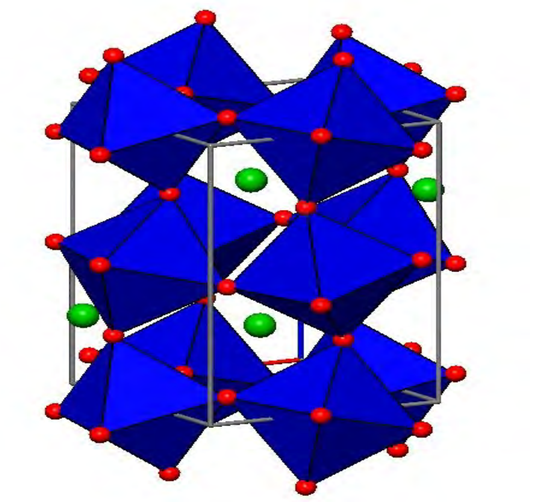

Merkel *et al*, in prep.

pPv to Pv, 900 K – Grain Orientations

$NaCoF_3$ post-perovskite

Before Transformation

P = 17.5 GPa – T = 900 K

Fine matrix:	68 %
Extracted spots:	4715
Indexed spots:	62 %
Indexed grains:	1317

$NaCoF_3$ Perovskite

After Transformation

P = 12.5 GPa – T = 900 K

Fine matrix:	4 %
Extracted spots :	17635
Indexed spots:	60 %
Indexed grains:	271

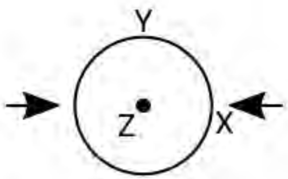

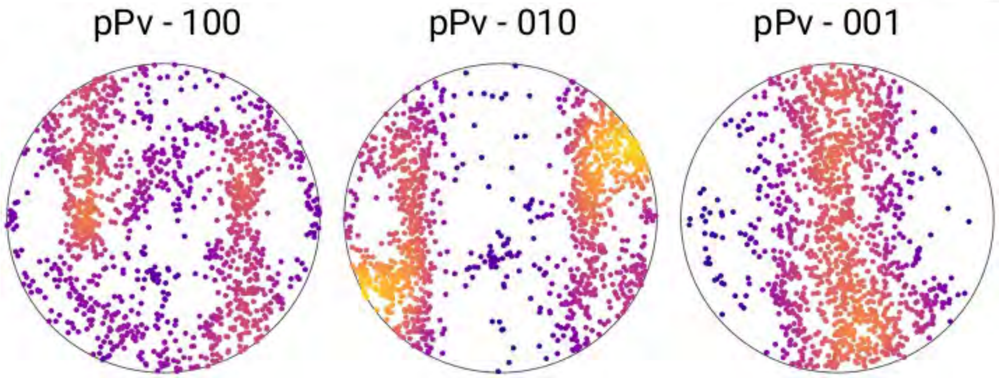

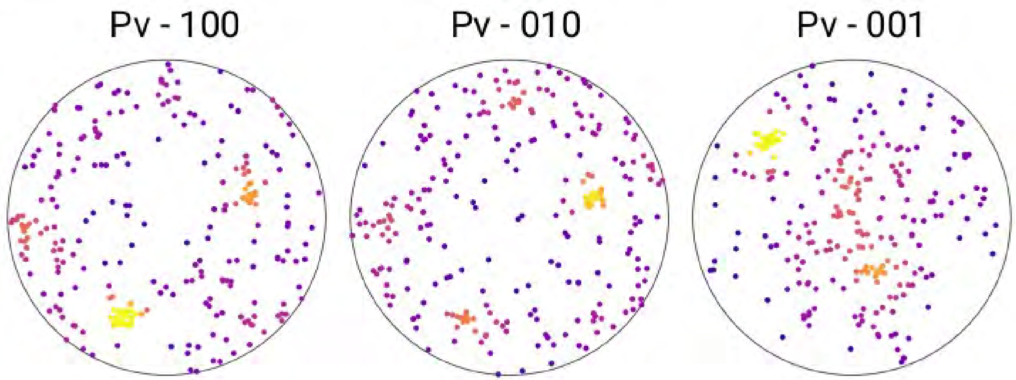

Take home messages

Orientation memory
Dobson-like mechanism
Grain size divided by ~ 2

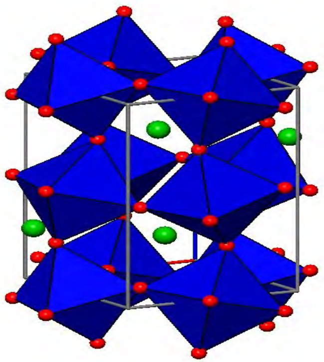

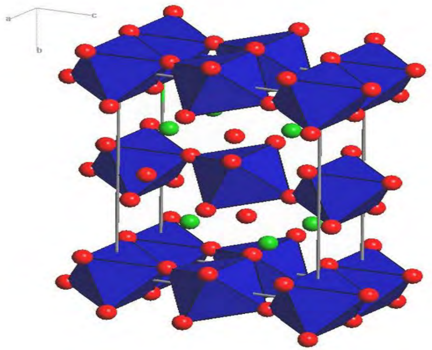

$NaCoF_3$ Perovskite

$NaCoF_3$ post-Perovskite

No orientation memory
Nucleation and growth dominated
Grain size multiplication (x10?)

On Pv and pPv in D"

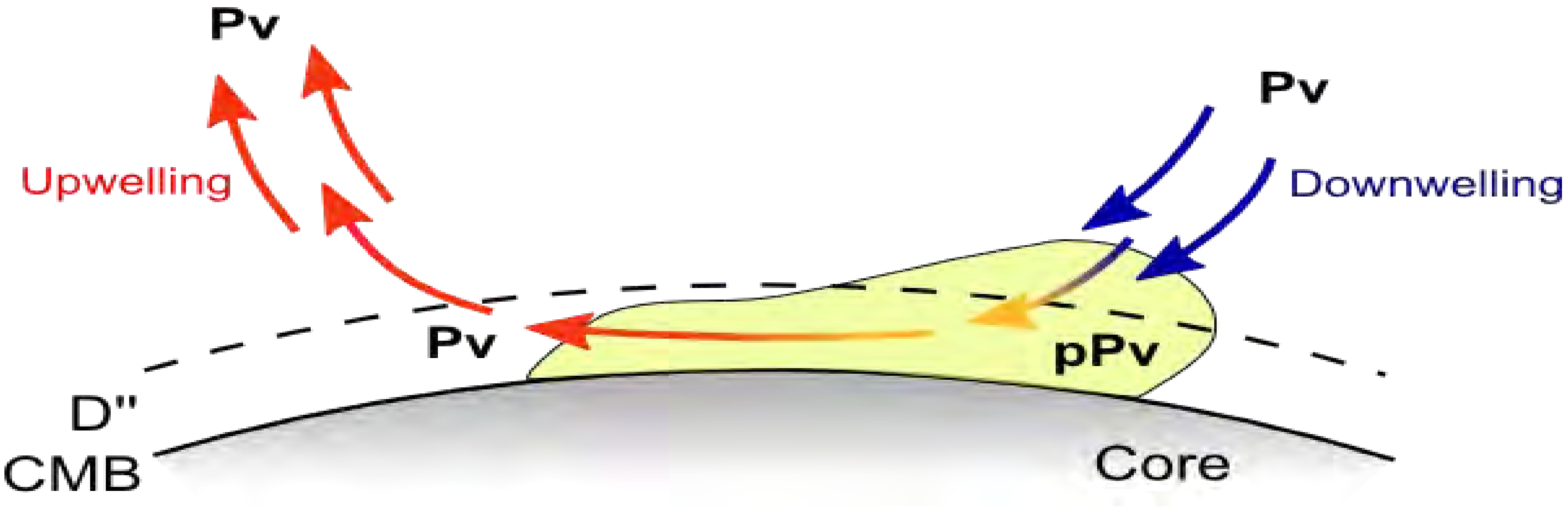

On Pv and pPv in D''

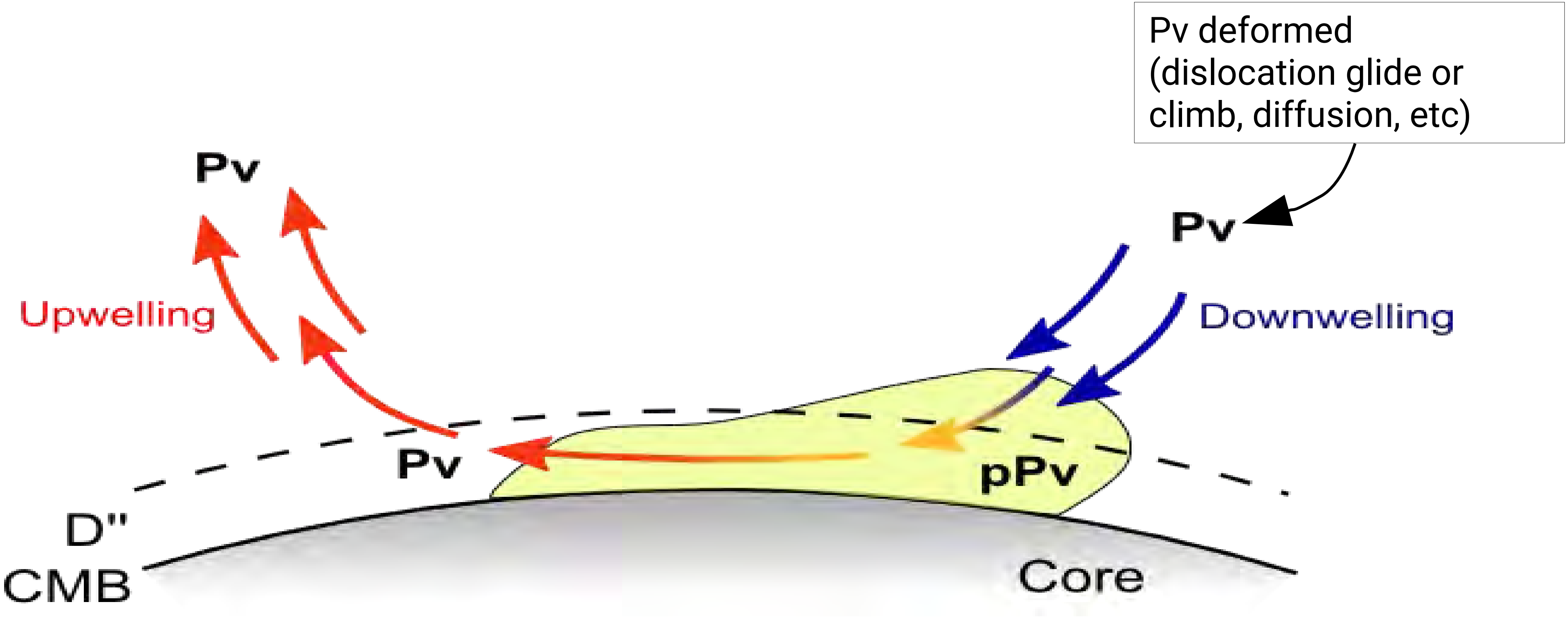

On Pv and pPv in D''

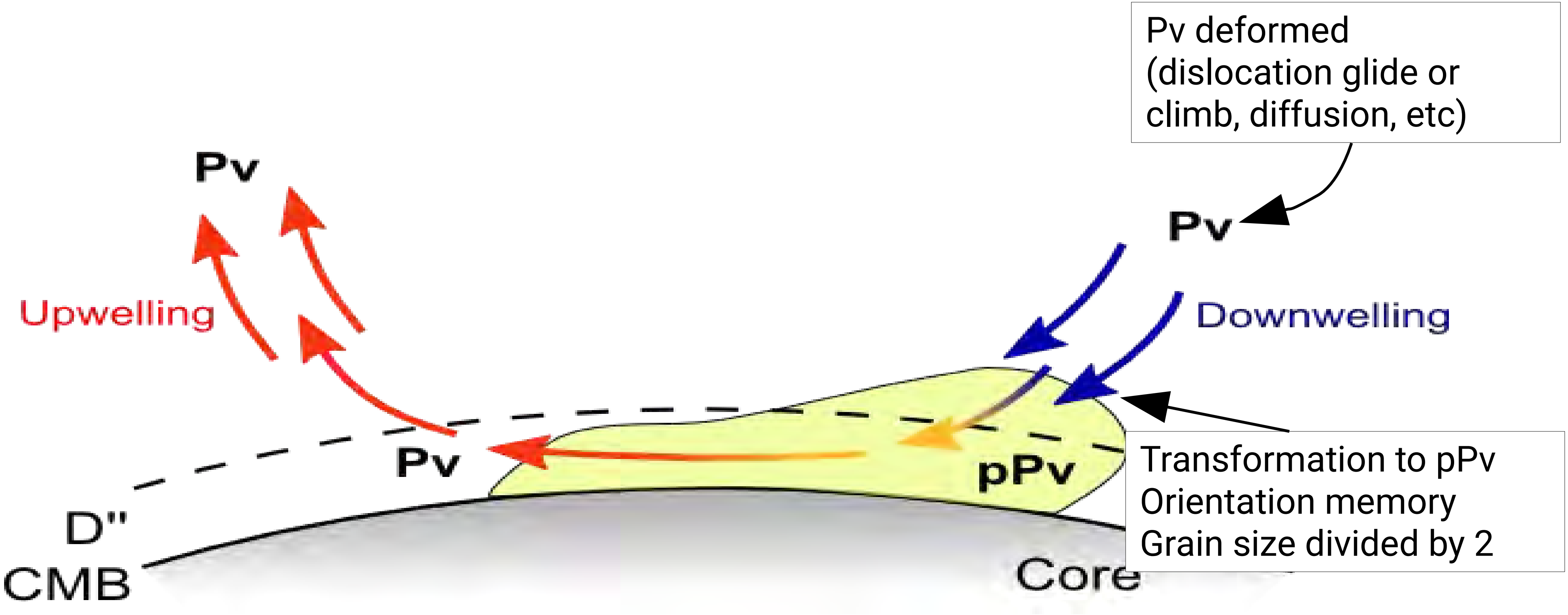

On Pv and pPv in D''

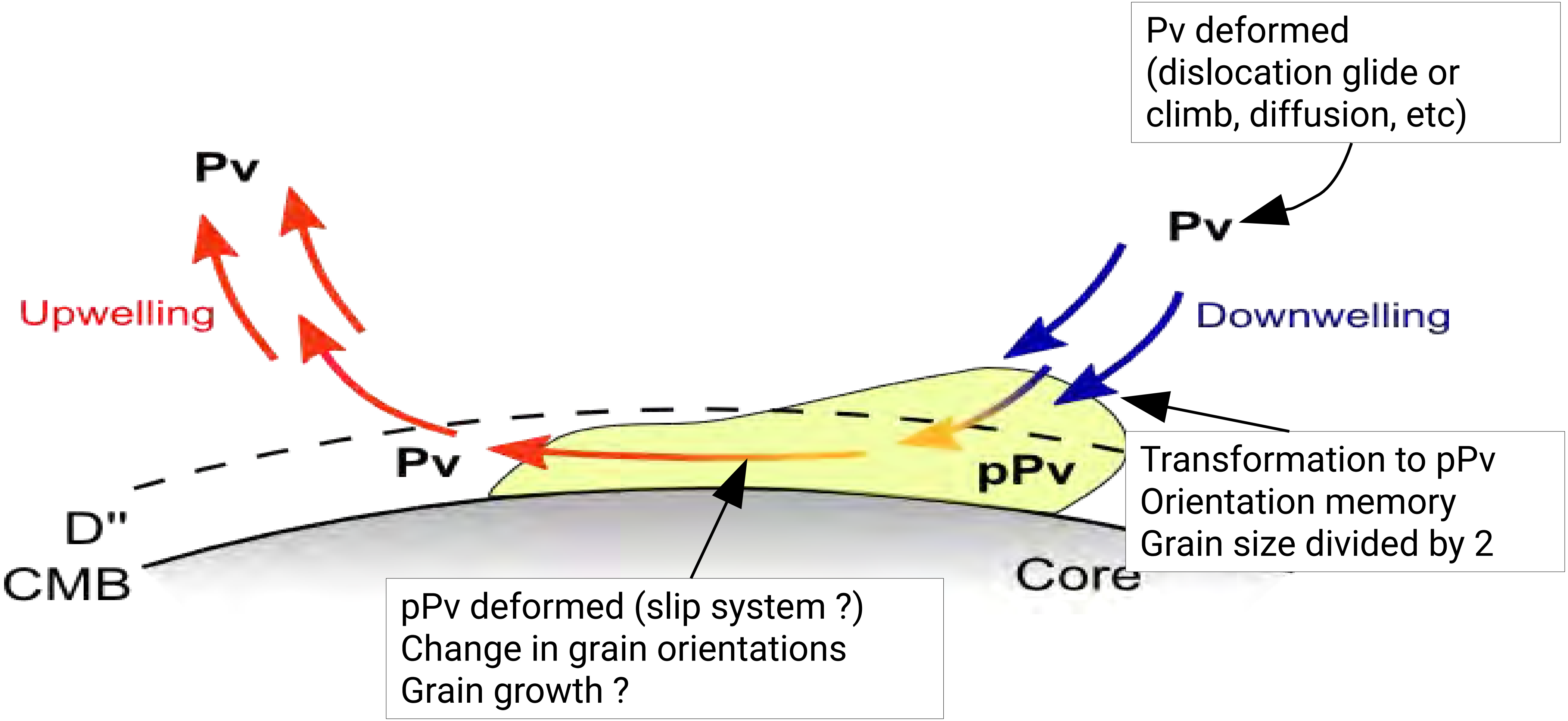

On Pv and pPv in D"

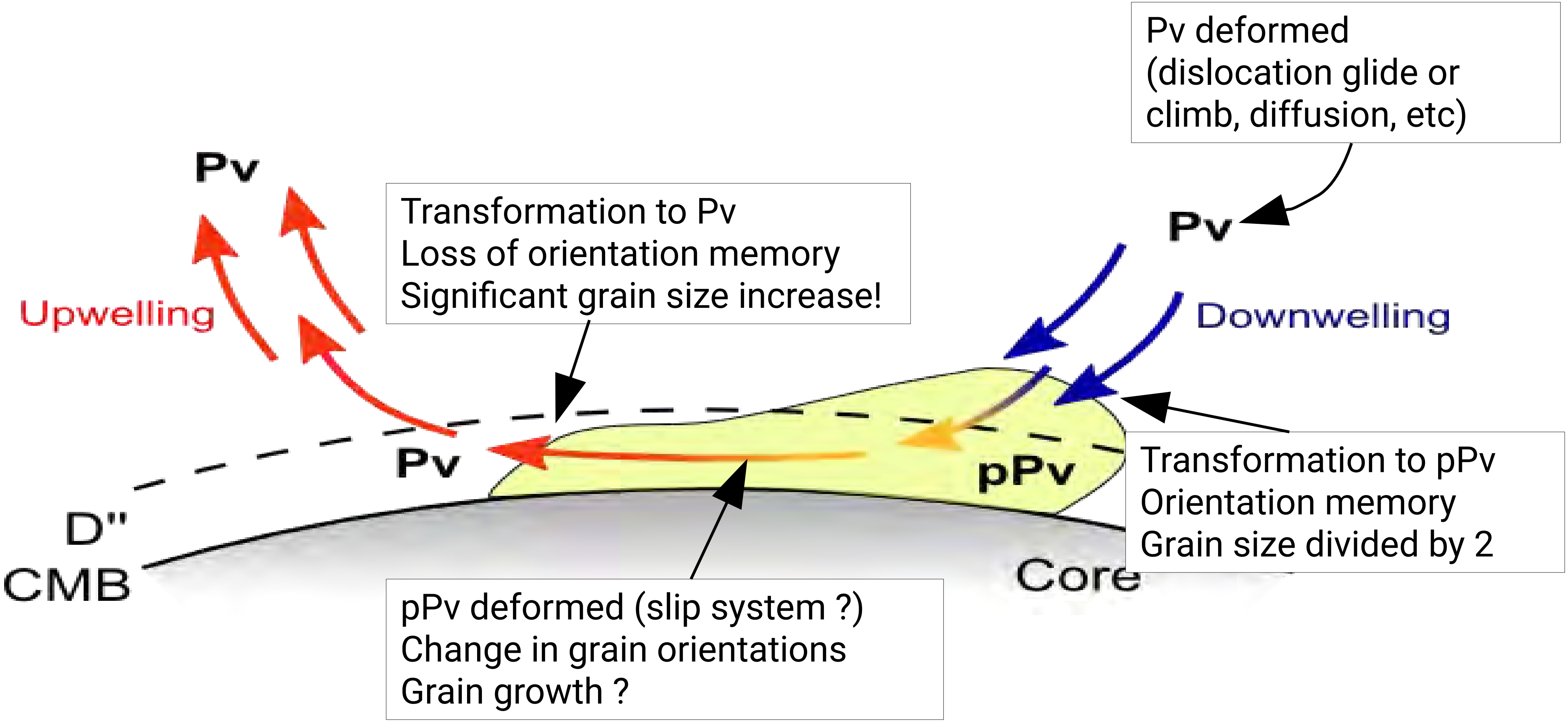

On Pv and pPv in D''

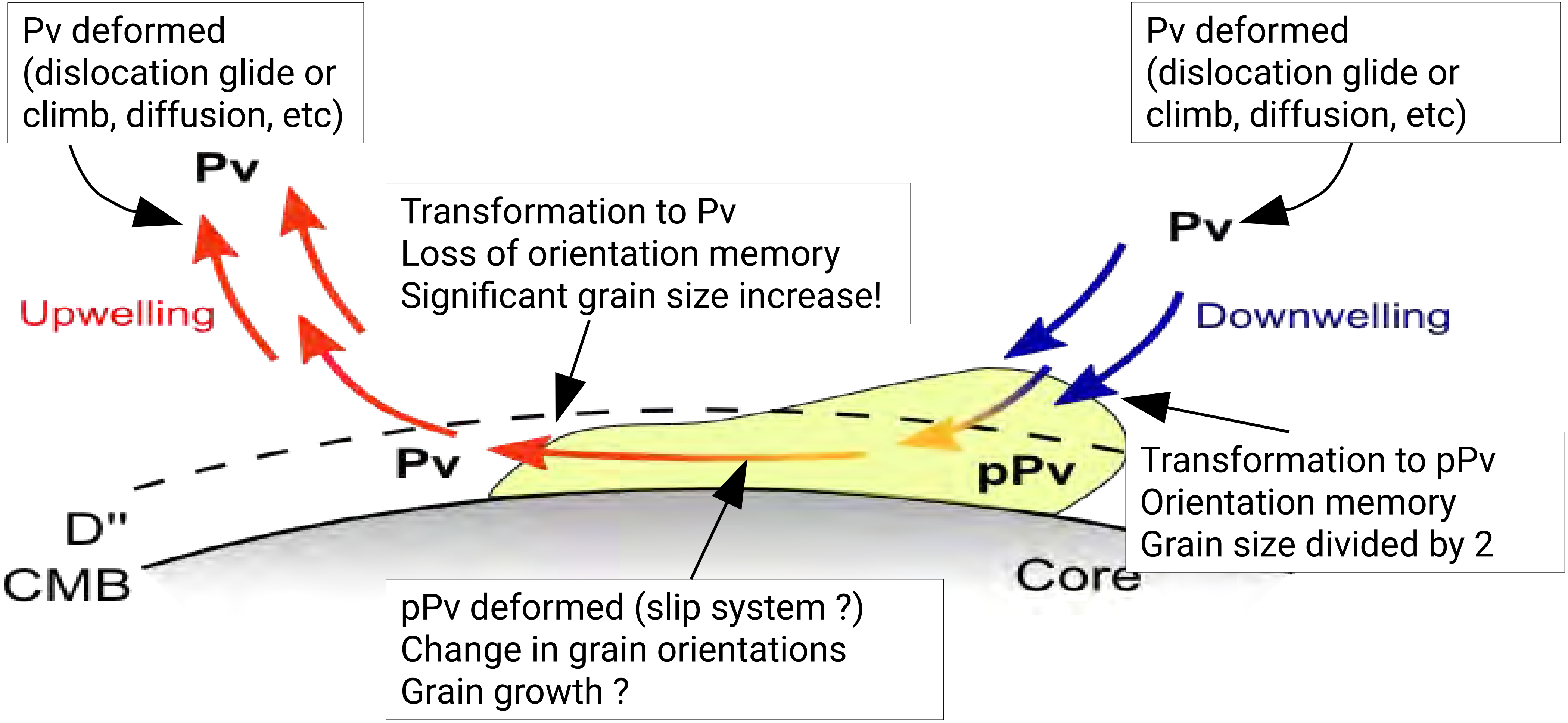

Perspective: microstructural studies along a deep mantle geotherm

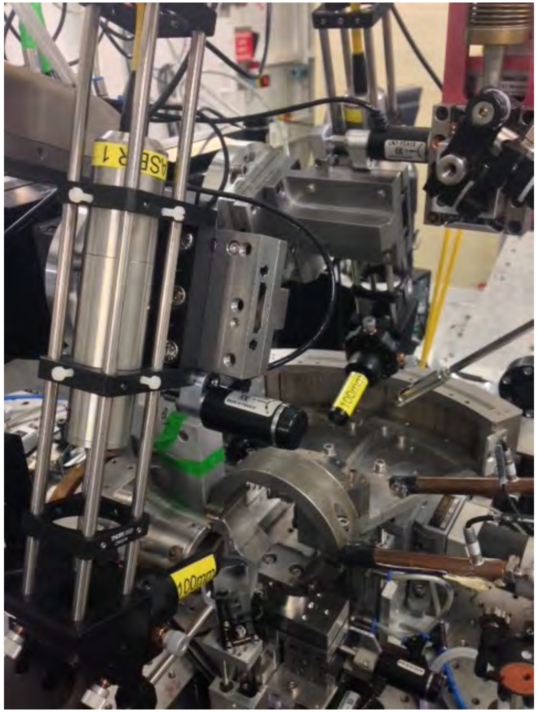

Combining multigrain crystallography and in-situ laser-heating in the DAC

Perspective: microstructural studies along a deep mantle geotherm

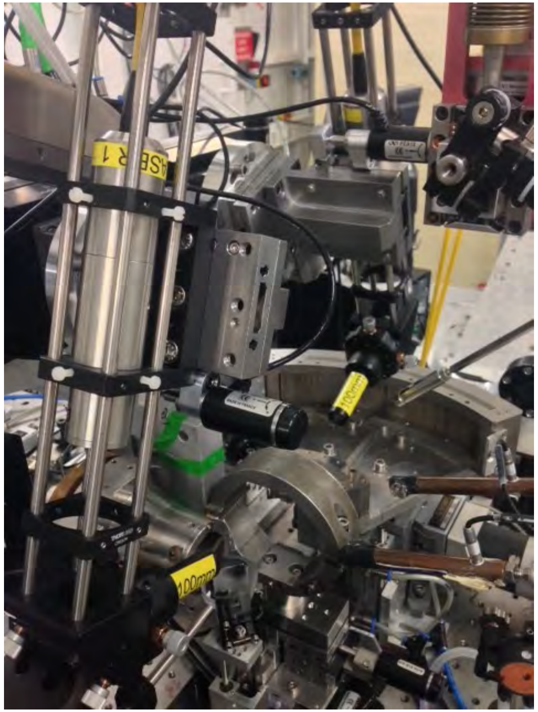

Combining multigrain crystallography and in-situ laser-heating in the DAC

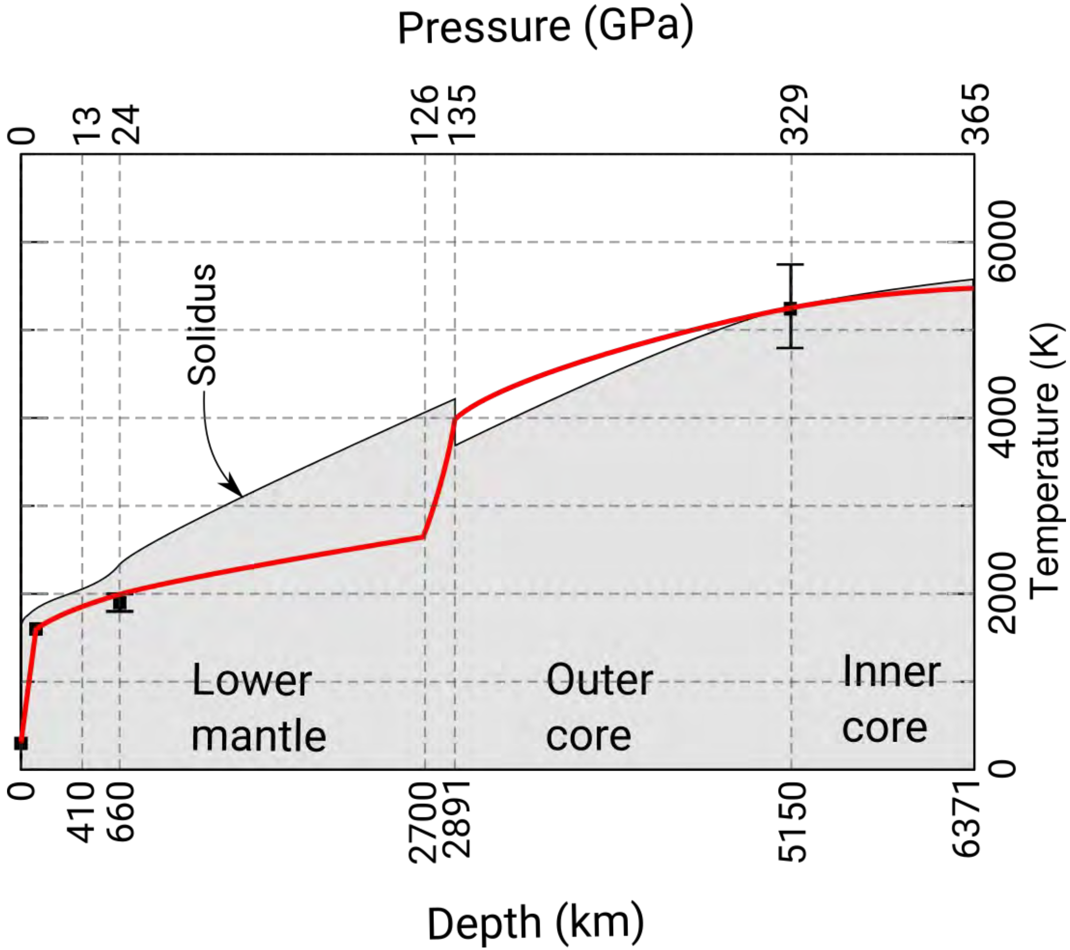

Perspective: microstructural studies along a deep mantle geotherm

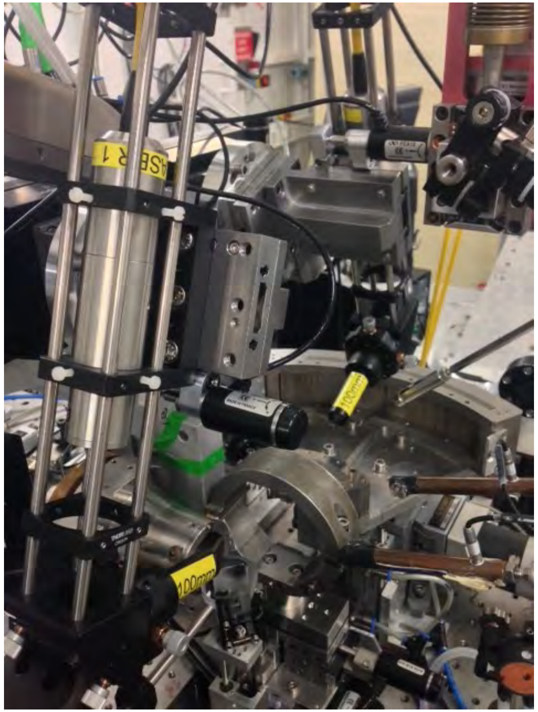

Combining multigrain crystallography and in-situ laser-heating in the DAC

Previous range of DAC def. experiments

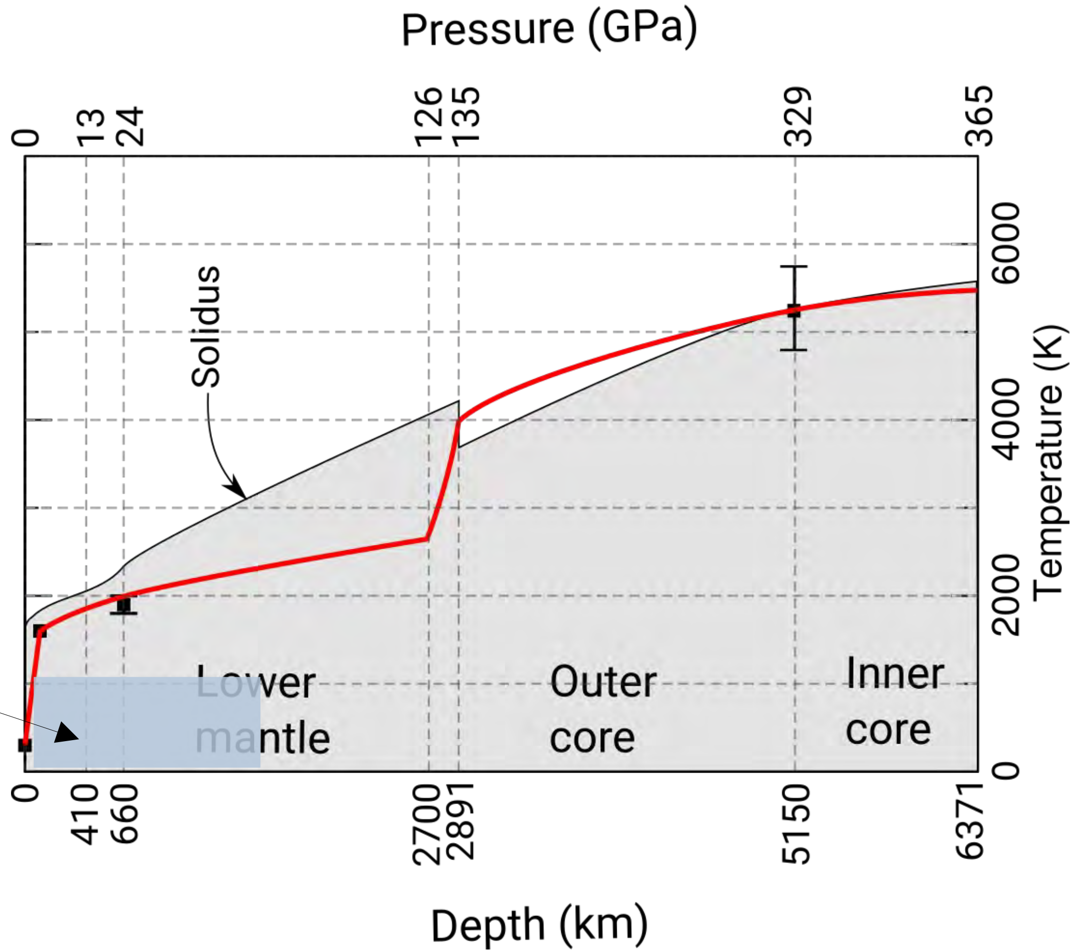

Perspective: microstructural studies along a deep mantle geotherm

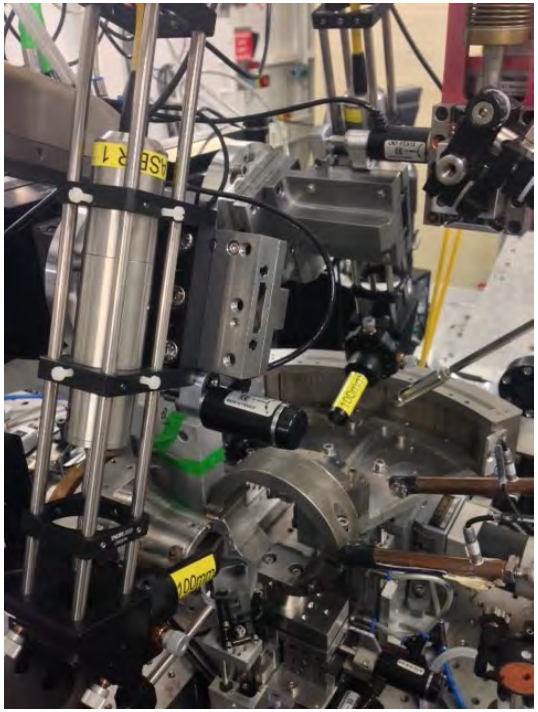

Combining multigrain crystallography and in-situ laser-heating in the DAC

Posters tonight

Previous range of DAC def. experiments

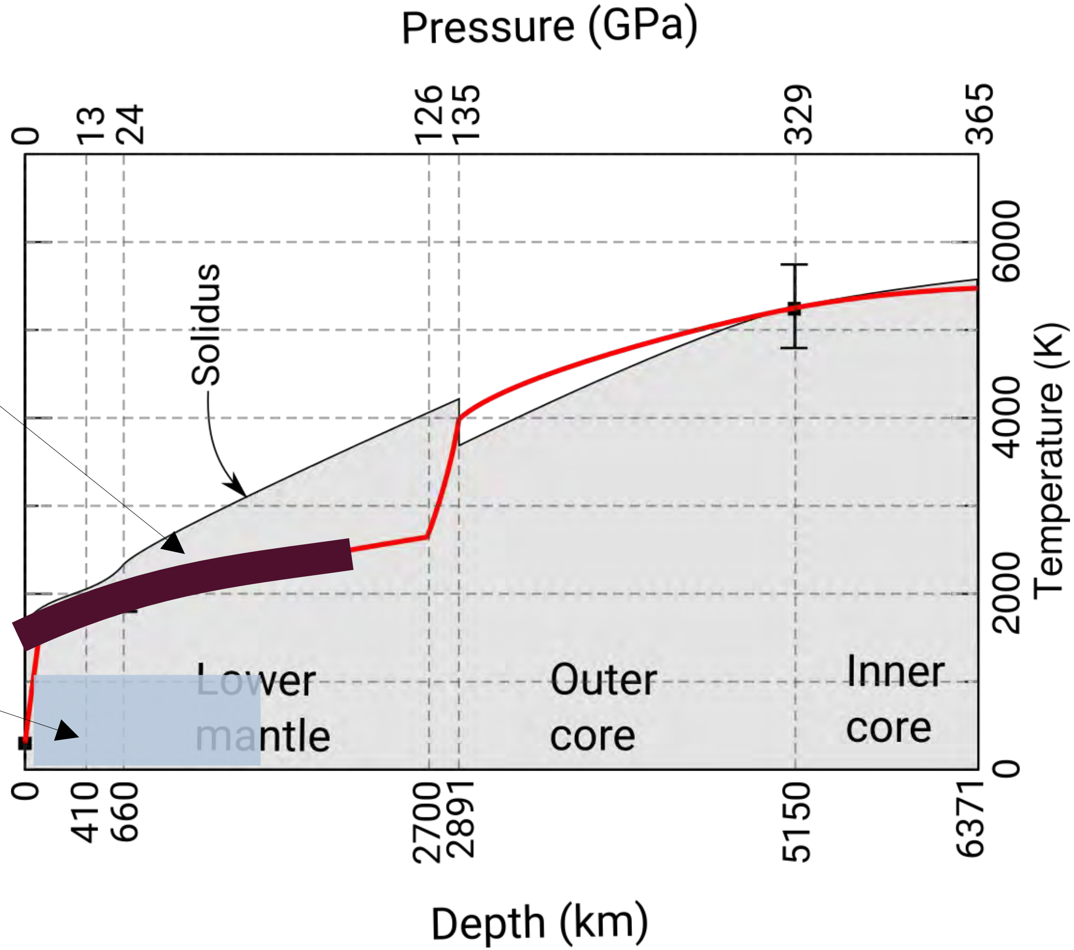

A primer: effect of water and temperature on anisotropy in wadsleyite

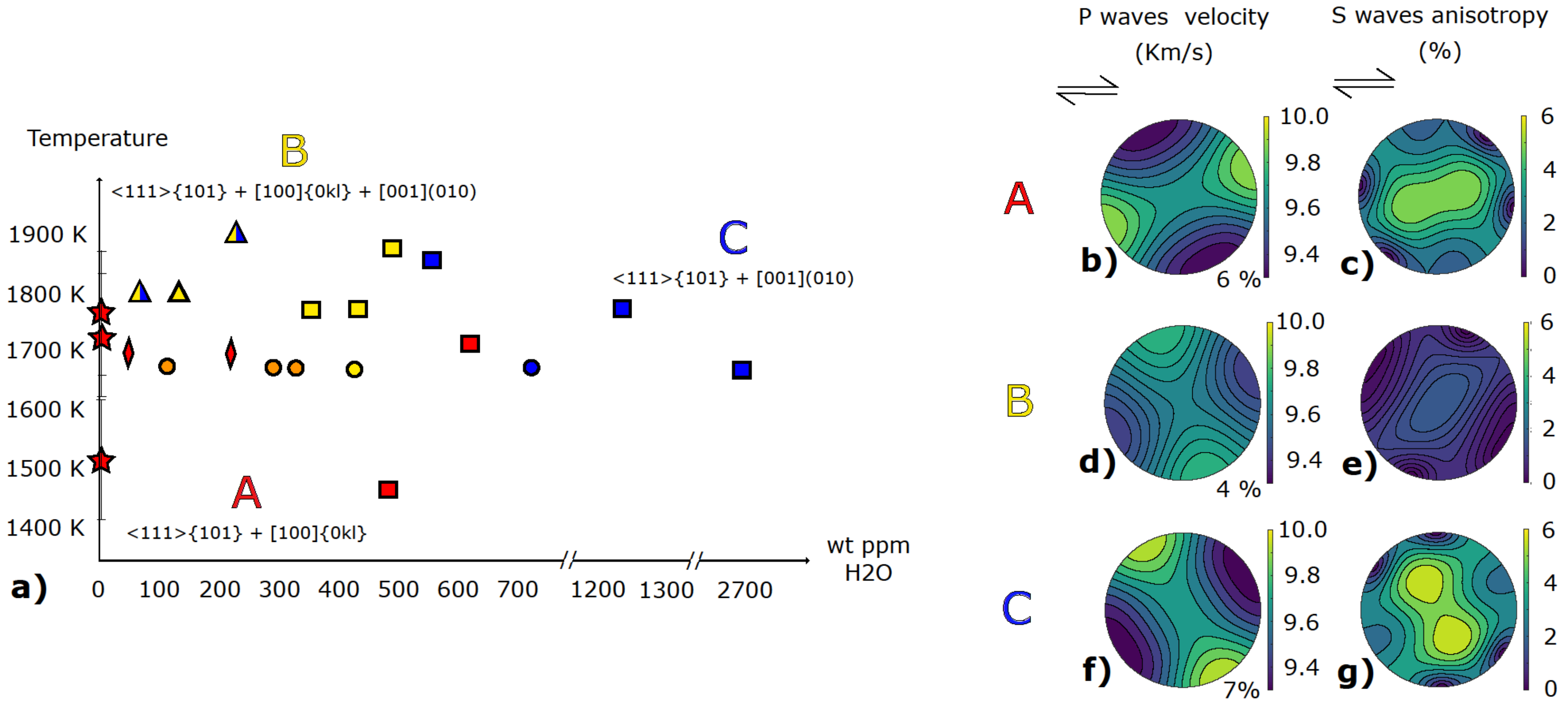

Phase transitions in the Earth’s mantle

Phase transitions in the Earth's mantle

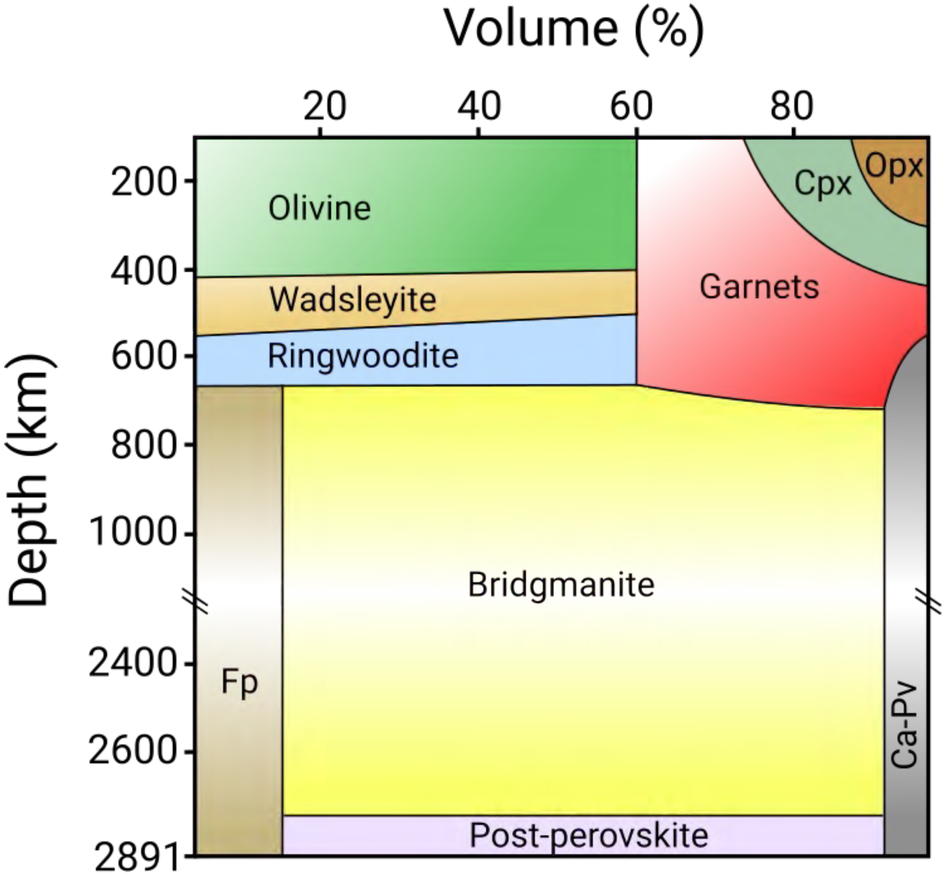

Cpx: clinopyroxene
Opx: orthopyroxene
Fp: ferro-periclase
Ca-Pv: calcium-perovskite

Phase transitions in the Earth's mantle

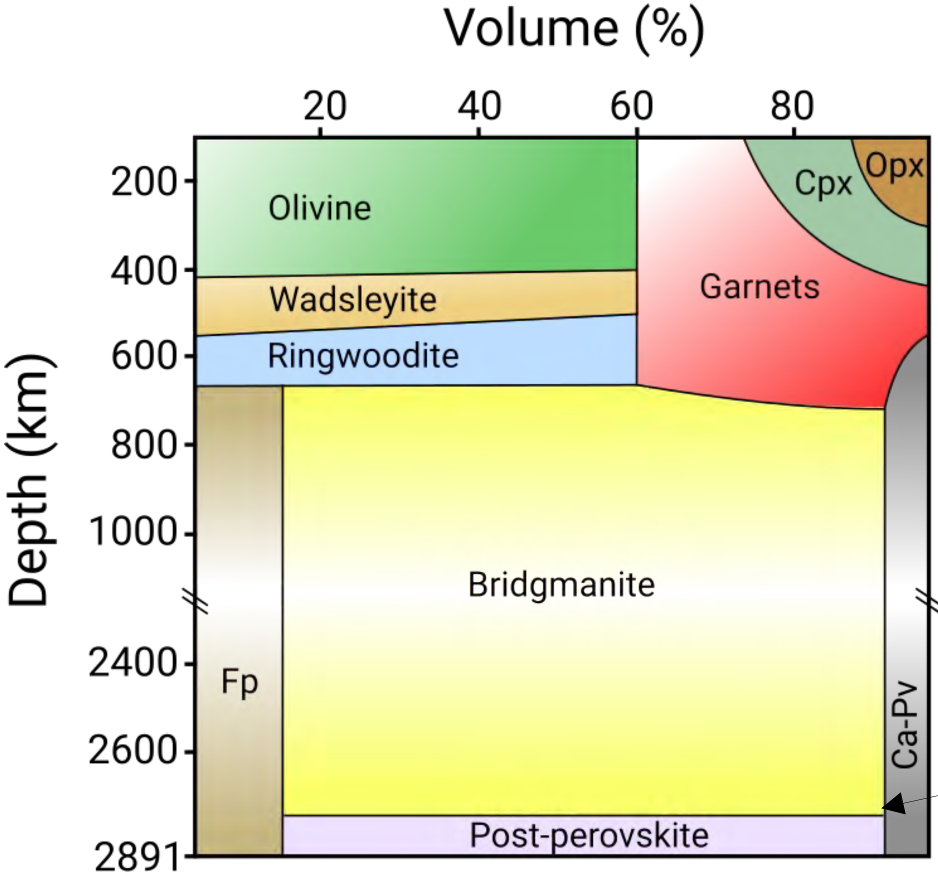

Cpx: clinopyroxene
Opx: orthopyroxene
Fp: ferro-periclase
Ca-Pv: calcium-perovskite

Detectability of the transition

- Effect of kinetics
- Dependence of wave period → thickness of Pv-pPv coexistence
- Amplitude of reflection → kinetics → temperature

Microstructures

- Texture memory at the Pv → pPv transition
- Loss of texture at the pPv → Pv transition

Phase transitions in the Earth's mantle

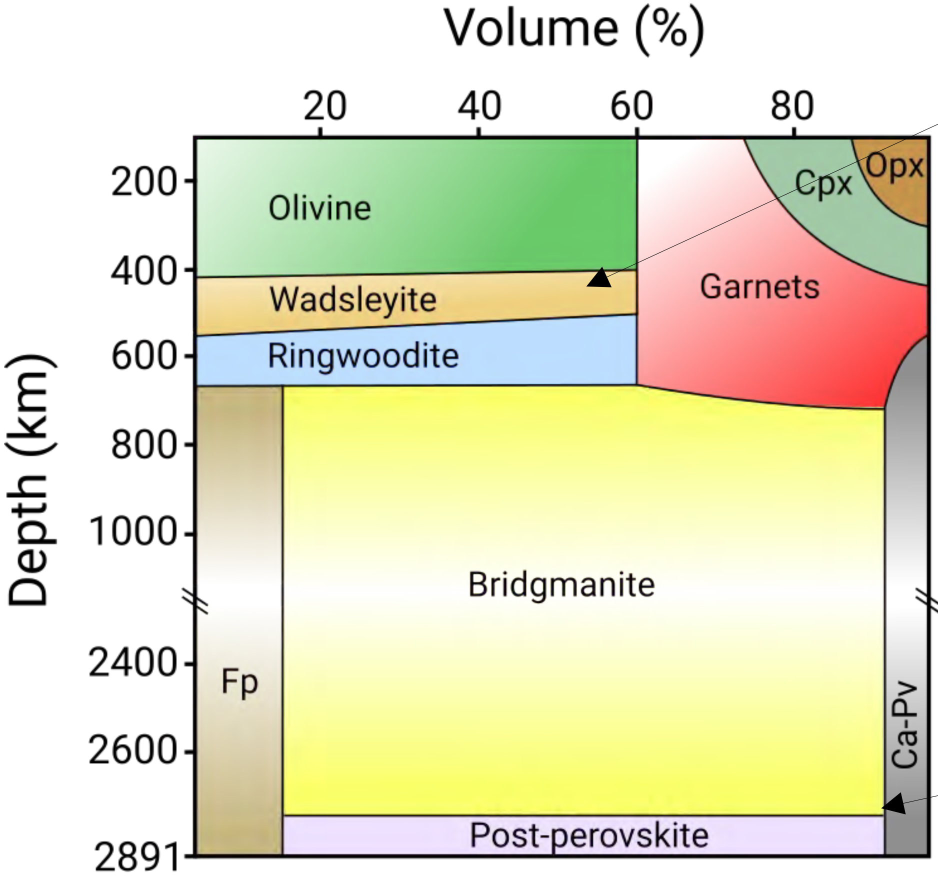

Cpx: clinopyroxene
Opx: orthopyroxene
Fp: ferro-periclase
Ca-Pv: calcium-perovskite

Poster of E. Ledoux later today
on wadsleyite and anisotropy in the transition zone

Detectability of the transition

- Effect of kinetics
- Dependence of wave period → thickness of Pv-pPv coexistence
- Amplitude of reflection → kinetics → temperature

Microstructures

- Texture memory at the Pv → pPv transition
- Loss of texture at the pPv → Pv transition

Phase transitions in the Earth's mantle

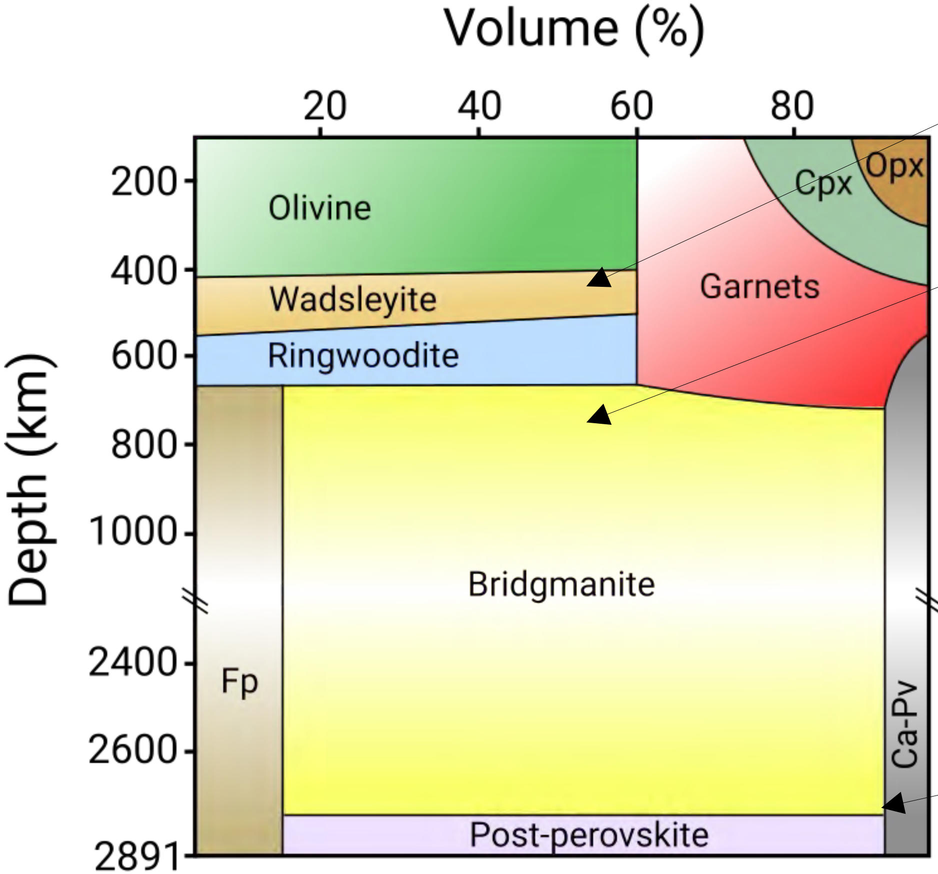

Cpx: clinopyroxene
Opx: orthopyroxene
Fp: ferro-periclase
Ca-Pv: calcium-perovskite

Poster of E. Ledoux later today
on wadsleyite and anisotropy in the transition zone

Poster of J. Gay later today
on bridgmanite and lower mantle

Detectability of the transition
- Effect of kinetics
- Dependence of wave period → thickness of Pv-pPv coexistence
- Amplitude of reflection → kinetics → temperature

Microstructures
- Texture memory at the Pv → pPv transition
- Loss of texture at the pPv → Pv transition